AD NUMBER
AD379809
CLASSIFICATION CHANGES
TO: **UNCLASSIFIED**
FROM: **CONFIDENTIAL**
LIMITATION CHANGES
TO: **Approved for public release; distribution is unlimited.**
FROM: **Distribution authorized to U.S. Gov't. agencies and their contractors; Critical Technology; MAR 1966. Other requests shall be referred to Air Force Rocket Propulsion Laboratory, Research and Technology Division, Edwards AFB, CA. This document contains export-controlled technical data.**
AUTHORITY
31 MAR 1979, dodd 5200.10 gp-4; AFRPL ltr dtd 20 Dec 1985

AD 379 809

AUTHORITY: AFRPL
ltr 20 DEC 85

SECURITY MARKING

The classified or limited status of this report applies to each page, unless otherwise marked.
Separate page printouts MUST be marked accordingly.

THIS DOCUMENT CONTAINS INFORMATION AFFECTING THE NATIONAL DEFENSE OF THE UNITED STATES WITHIN THE MEANING OF THE ESPIONAGE LAWS, TITLE 18, U.S.C., SECTIONS 793 AND 794. THE TRANSMISSION OR THE REVELATION OF ITS CONTENTS IN ANY MANNER TO AN UNAUTHORIZED PERSON IS PROHIBITED BY LAW.

NOTICE: When government or other drawings, specifications or other data are used for any purpose other than in connection with a definitely related government procurement operation, the U. S. Government thereby incurs no responsibility, nor any obligation whatsoever; and the fact that the Government may have formulated, furnished, or in any way supplied the said drawings, specifications, or other data is not to be regarded by implication or otherwise as in any manner licensing the holder or any other person or corporation, or conveying any rights or permission to manufacture, use or sell any patented invention that may in any way be related thereto.

AFRPL-TR-67-78

(Unclassified Title)

ADVANCED THRUST CHAMBER FOR SPACE MANEUVERING PROPULSION

Third Quarterly Report

H. G. Diem

Rocketdyne
A Division of North American Aviation, Inc.
Canoga Park, California

Technical Report AFRPL-TR-67-78

March 1967

Air Force Rocket Propulsion Laboratory
Research and Technology Division
Edwards Air Force Base, California
Air Force Systems Command
United States Air Force

AFRPL-TR-67-78

(Unclassified Title)

ADVANCED THRUST CHAMBER FOR SPACE MANEUVERING PROPULSION

Third Quarterly Report

H.G.Diem

Air Force Rocket Propulsion Laboratory
Research and Technology Division
Edwards Air Force Base, California
Air Force Systems Command
United States Air Force

FOREWORD

(U) This third Quarterly Report describes the progress made in the Advanced Thrust Chamber for Space Maneuvering Propulsion Program, Tasks II and III, during the period of 16 November to 15 February 1967, and is submitted in accordance with the requirements of Contract AF04(611)-11617.

(U) This publication was prepared by Rocketdyne, a Division of North American Aviation, Inc., as report R-6727-3.

(U) Publication of this report does not constitute Air Force approval of the report's findings or conclusions. It is published only for the exchange and stimulation of ideas.

W. W. Wells, AFRPL Program Manager, RPREC

UNCLASSIFIED ABSTRACT

(U) Hardware design, fabrication, and hot-firing test results for solid-wall toroidal thrust chamber segments and the tube-wall nozzle inserts are discussed. Solid-wall segment testing was conducted to evaluate injector and thrust chamber contour designs with respect to performance and heat transfer. Analysis, design and fabrication of tube-wall throat inserts, tube-wall segments, and structural test segments are presented.

CONTENTS

ILLUSTRATIONS

TABLES

SECTION I
INTRODUCTION

(C) A study under sponsorship of AFRPL, was conducted during the 1965 calendar year to define an advanced optimized liquid fluorine/liquid hydrogen (LF_2/LH_2) space maneuvering propulsion system (Contract AF04(611)-10745). The mission of primary interest, which defined the propulsion system requirements, was that of intercept and rendezvous with passive and evasive target satellites.

(C) The study resulted in defining an optimum engine configuration utilizing concentric thrust chambers. The outer primary thrust chamber of 30,000 pounds thrust incorporated the toroidal-aerodynamic spike design concept. The inner secondary thrust chamber of 3300 pounds thrust was of a bell-type nozzle design.

(U) Because of the potential mission performance capability gains of this propulsion system concept, the present study was undertaken to verify the critical design features of this concept. The toroidal-aerospike thrust chamber is the unique concept, and is the primary basis for the engine design. Therefore, demonstration effort was concentrated in this area.

(C) An additional task of the current program was to extend the system studies of Contract AF04(611)-10745 to determine the mission performance capabilities of larger gross weight space maneuvering vehicles. Also, for the 20,000-pound gross weight vehicles defined previously in Contract AF04(611)-10745, the orbital life capabilities beyond the previously established requirement of 14 days were to be determined. The results of these studies were reported separately as a final report (Ref. 1).

(U) The basic objective of the present experimental program is to demonstrate the critical features associated with operating the toroidal thrust chamber, while delivering high performance, at the operating parameters defined by the studies of Contract AF04(611)-10745. The specific objectives of the program are as follows:

1. Demonstrate high combustion efficiency over the throttling range
2. Determine the effect of chamber contour and injector characteristics on performance and heat flux distribution
3. Demonstrate the feasibility of supplying temperature-controlled chamber tapoff gas (simulating turbopump requirements) by regulating the local injector mixture ratio distribution
4. Demonstrate the ability to regeneratively cool the chamber
5. Demonstrate that the lightweight support structure can maintain the nozzle throat size within an acceptable tolerance

(C) The approach to the experimental program is to test a full-size segment of the complete toroidal chamber. The segment is 3 inches in length representing approximately 1/47 of the complete toroid circumference. Previous testing has shown that combustion and heat transfer results from segments of this size duplicate those obtained with the complete 360-degree toroid. Segment testing permits obtaining the desired test data at reduced hardware costs and with relative experimental ease.

(U) This philosophy is implemented by the building-block concept illustrated in Fig. 1. The first three objectives were accomplished using solid-wall, water-cooled hardware. Using these relatively inexpensive components, the injector and thrust chamber configurations are optimized. Heat transfer results in the throat region are verified using the hydrogen-cooled nozzle sections shown in Fig. 1. These inserts are water-cooled on one side to obtain additional heat transfer data and are interchangeable with the completely water-cooled nozzle sections.

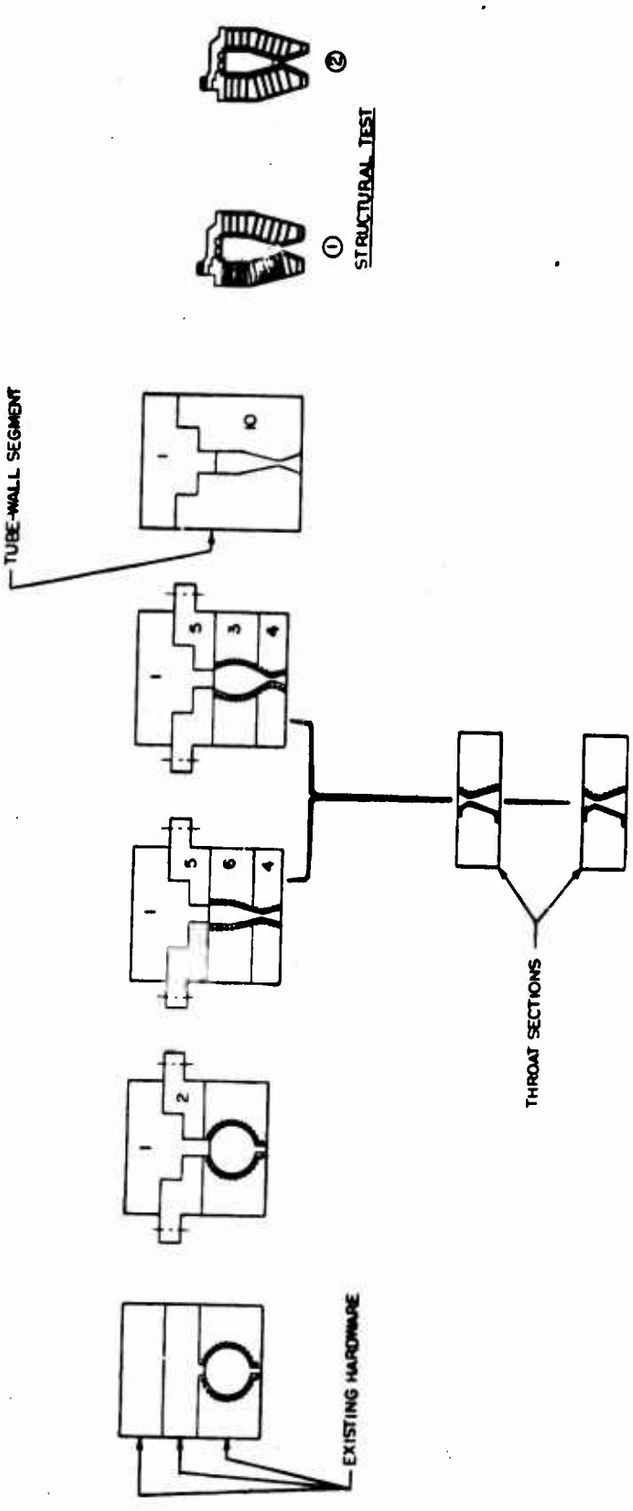

Figure 1 . Test Hardware Interchangeability

(U) Following the throat insert testing, completely regeneratively cooled thrust chamber segments are tested using the same type injector as in the previous segments. Concurrently, two lighweight segments shown in Fig. 1 will be built and pressure tested to demonstrate the structural integrity of the concept. These segments will differ from each other in that a rib-type backup structure will be used on one segment, while for the other segment, honeycomb support structure will be used on one side.

(U) During the first quarter of the program (Ref. 2), the extended system studies (Task I) were completed. Facility modifications were accomplished and segment hardware was designed and fabricated for the test program. The initial contour and injector-characteristics evaluation tests were conducted. Analyses were conducted to determine the structural configuration of the thrust chamber, and the basic design for the tube-wall nozzle insert was completed.

(U) During the second quarter, contour and injector characterization tests were continued with the solid-wall hardware. Injector mixture ratio bias tests were also conducted. Design of tube-wall throat inserts using CRES and nickel tubes was completed and fabrication of the inserts was initiated. Design release for the tube wall and structural segments was also initiated. These results are reported in Ref. 3.

SECTION II
SUMMARY

(C) During the third quarter, the Task II, Solid-Wall Segment Evaluation, effort was completed. Hot gas injector tapoff tests were conducted which demonstrated the insensitivity of tapoff gas temperature to throttling ratio(chamber pressure). The test results also indicated that high injector efficiency could be maintained. The injector mixture ratio bias test series was completed. The results of this test series indicated that some reduction of the throat heat transfer rate could be affected but that redesign of the injector elements would be required to regain performance. Incorporation of engine base pressure effects and thrust recalibration has resulted in close correlation between the C* performance values based on chamber pressure with those based on thrust.

(C) The tube-wall throat inserts were fabricated during the report period and facility modifications to test these components were completed. Five tests were conducted or the CRES tube at chamber pressures ranging from 291 to 642 psia. On the last test, the tubes were eroded during a chamber pressure overshoot to 835 psia which resulted from an improperly sequenced facility LF_2 valve. A flow check of the nickel tube-wall insert showed high pressure drops in the hydrogen coolant tubes. Examination of the tubes indicated a closely packed crystalline substance but no evidence of tube constriction.

(C) Fabrication of the tube-wall segments continued. Two identical segments are being fabricated using constant outside diameter, variable inside diameter nickel tubes. The tubes are electron beam welded into flat tube bundles and then formed to the contour of the combustion chamber and nozzle. A modification of the contour and the tube distribution (tubes/pass) was made to provide improved coolant system operation.

(C) Fabrication of the structural test segments was initiated. Electron beam welding of the channels for the rib structure is being used to provide a lightweight, uniform weld. The method was selected after samples of EB and TIG welded channels were evaluated. A 21-inch, three-compartment rib structural segment is being fabricated with a detachable outer wall.

(U) Analytical studies indicated that an outer wall of honeycomb could be tested with the inner wall of the rib structural segment to provide data which could be used to accurately determine the throat area variations in a complete honeycomb segment which would result from chamber pressure induced forces.

(U) Prior to starting the fabrication of the honeycomb segment, a fabrication-techniques demonstration was performed to verify all critical processes involved in the honeycomb segment fabrication. These processes included welding of thin-sheet honeycomb to the baffles and injector and brazing the interior and exterior face sheets to the honeycomb core. After the proper procedures were developed and materials selected, fabrication of the honeycomb segment was initiated and has progressed to the point where completion is anticipated simultaneously with the completion of the mechanical tests of the rib structural segment.

SECTION III

TASK II SOLID-WALL SEGMENT EVALUATION

(C) The solid-wall, water-cooled segment evaluation effort was completed during this quarter. A total of 130 tests was conducted with this hardware to date to evaluate the effects of injector and chamber configuration on heat transfer and performance characteristics of the segment. During the report period, tests were conducted to demonstrate the feasibility of drawing hot gases for turbine operation from the thrust chamber through the injector and to show the effects of injector mixture ratio bias. A detailed summary of the test results is presented in Appendix A. Other contours in addition to the three shown in Fig. 1 were built and tested. The characteristics of these contours are reviewed in Table I. Most of the hardware had been designed and fabricated during the previous quarter.

TABLE I

(C) THRUST CHAMBER CONTOUR CHARACTERISTICS

Contour	Injector-Throat Distance, inches	Nominal Convergence Angle, degrees	Maximum Contraction Area Ratio	Contour Wall Shape
A	3.5	60	18	Circular
B	3.5	30	12	Curved
C	3.5	30	7	Straight
D	5.0	15	7	Straight
E	3.5	15	7	Straight

1. HOT GAS TAPOFF DEMONSTRATION

(C) Engine fabrication and operation can be simplified by eliminating the conventional gas generator and using hot gases tapped from the combustion chamber as the turbine driving fluid. These gases may be tapped from the vicinity of the combustion chamber wall or from the injector. The construction of the injector is such that obtaining tapoff gases from this source appeared the most feasible. Thrust chamber gas tapoff was considered as an alternate, but this concept was not investigated because of the highly successful results obtained with the injector tapoff configuration.

(C) The purpose of the tests was to demonstrate (1) structural integrity of the injector while withdrawing hot gases through the injector face; (2) that combustion chamber performance is not strongly affected by this method of obtaining tapoff gas, and (3) that the tapoff gas properties are reasonably constant at all thrust levels.

(C) The injector tapoff evaluation was conducted with a Contour E chamber configuration. To conserve hardware, the two-row triplet injector was used which had previously been modified for the injector characterization studies reported in Ref. 3 . This injector therefore had 0.055-inch-diameter GH_2 orifices compared with the nominal value of 0.037 inches. The performance of this injector without tapoff, was 97 percent when used with the Contour E chamber. The injector, modified for tapoff, is shown in Fig. 2 . A hot-gas tapoff tube is inserted through the back of the injector and sealed at that location. The tube continues through the hydrogen-injection manifold and partially through a hole in the injector face. The injector-face hole is larger in diameter than the tapoff tube which is centered in the hole by three lands.

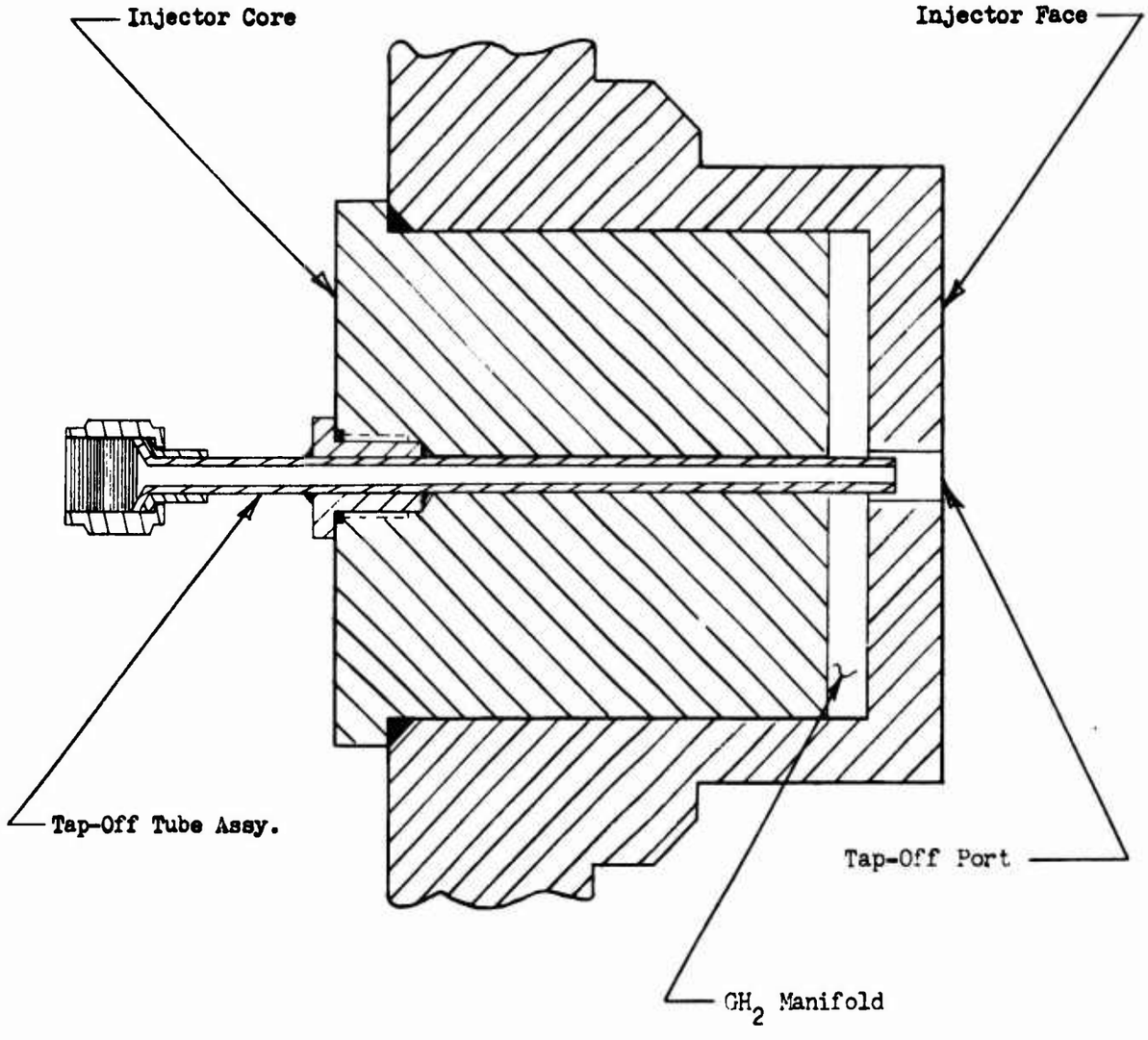

Figure 2 . Injector Tapoff Configuration

(C) In this configuration, the combustion chamber hot gases are mixed with the GH_2 flowing through the annular gap between the tapoff tube and injector body. The combined gases then flow through the center of the tapoff tube. The temperature of the tapoff gas depends upon the width of the annular gap and position of the end of the tapoff tube with respect to the injector face. As the tapoff tube is retracted behind the injector face, a greater percentage of hydrogen from the manifold enters the tapoff tube and the tapoff gas mixture ratio and final temperature is reduced. Increasing the annular gas gap also results in more GH_2 entering the tapoff tube relative to the amount of combustion chamber gas entering. However, as the gap is increased, more hydrogen flows into the combustion chamber through the gap, thus affecting the injector mixture ratio distribution and possibly affecting performance.

(U) This injector tapoff configuration results in substantially constant tapoff gas mixture ratio because the hydrogen manifold pressure is almost directly proportional to chamber pressure. The variation of tapoff gas temperature and molecular weight with mixture ratio is shown in Fig. 3 .

(U) The facility and instrumentation items used for the tapoff test series are shown schematically in Fig. 4 . The tapoff gas flows into an enlarged tube which serves as a plenum chamber for the sonic orifice located at the exit. The sonic orifice simulates the turbine nozzles or the turbine control valve, and therefore the sonic orifice is the flow-regulating device for the system. A series of thermocouples is installed along the length of the tube to verify that combustion has been completed prior to flowing through the sonic orifice. Measurement of the temperature, T, of the tapoff gas is used to determine the mixture

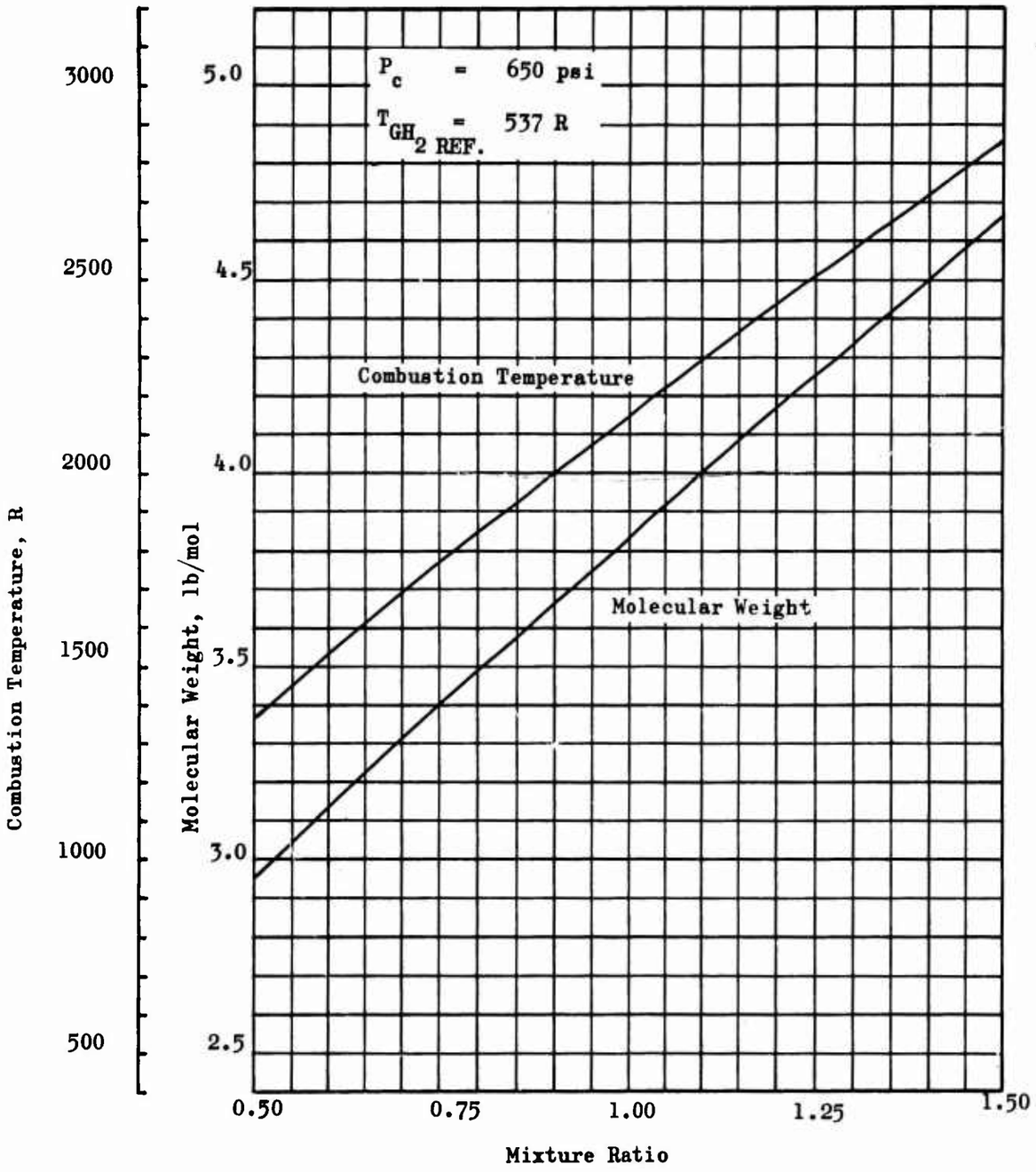

Figure 3 . Molecular Weight and Combustion Temperature for LF_2/GH_2

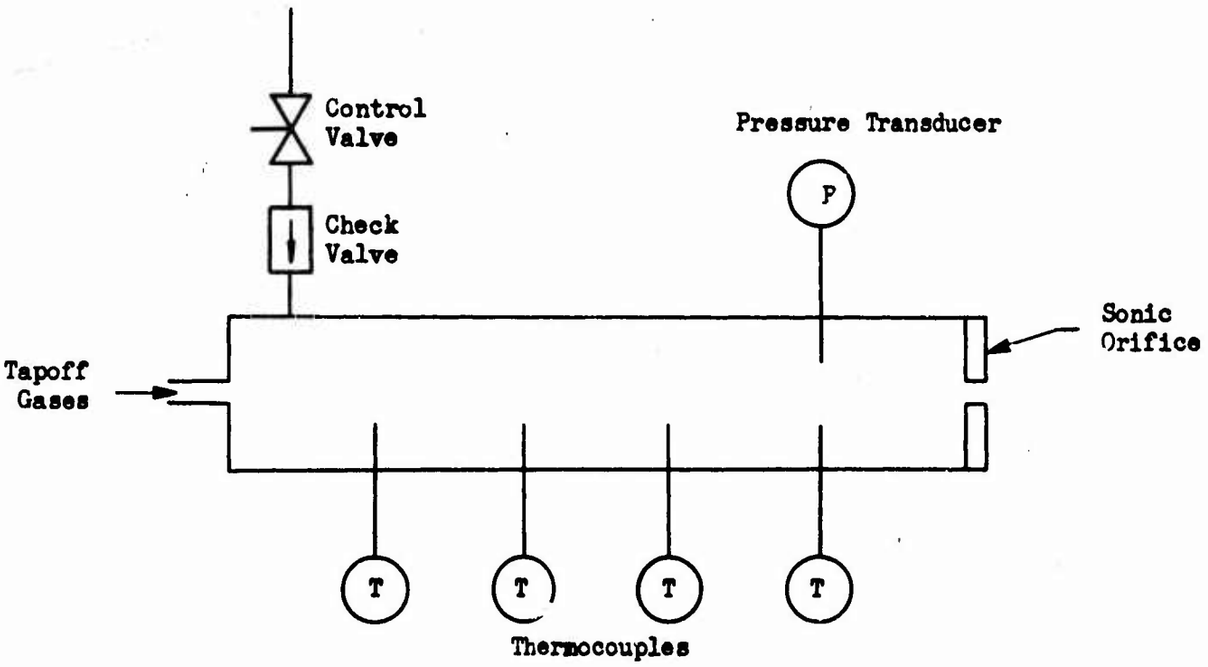

Figure 4 . Tapoff System Instrumentation Schematic

ratio and molecular weight, M, of the gas (based upon the gas properties shown in Fig. 3). For the relatively low temperatures and mixture ratios associated with tapoff gases, the molecular weight is nearly independent from pressure. The pressure measurement, P, is used in the following equation primarily to determine the flowrate, $\dot{w}$.

$$\dot{w} = KC_D AP(M/29T)^{\frac{1}{2}}$$

where K depends upon the specific heat ratio for the gas but is approximately 0.53 for the conditions tested. The discharge coefficient is C_D and the area of the sonic orifice is represented by A.

(U) The present tests were directed to investigate only steady-state operation because the actual transients will depend upon the configurations of several components not included in the test hardware; e.g., control valves and turbopump. A GN_2 purge is introduced into the plenum chamber and injector to eliminate transient off-mixture-ratio conditions at start. It was determined that the purge was improperly sequenced during the first three tests of this series.

(C) One of these tests was successful and resulted in a tapoff gas temperature of approximately 1600F. This was achieved with an annular gap of 0.006 inches and with the tapoff tube recessed 0.30 inches behind the injector face. On the two remaining tests, the tapoff tube burned. Analysis of the test data indicated the problem to be operational. The tapoff tube is purged during test start to prevent undesirable transients at that time. On the two unsuccessful tests, the purge had been terminated during the start transient. The purge termination was delayed until completion of start transition and no further difficulties thereafter were encountered.

(C) Because the temperature of the tapoff gases during the first test was based upon extrapolating transient data (a shielded thermocouple was used) it was decided to enlarge the annular gap to 0.012 inches. Three tests conducted with this gap size resulted in relatively low temperatures. The gap was then reduced to 0.009 inches and tested at chamber pressures ranging from 290 to 483 psia. The tapoff gas temperature varied from 940 to 1030F over this range of pressures. Test conditions and results are summarized in Table II.

(C) The heat transfer rates were not affected by the inclusion of the tapoff feature as indicated in Fig. 5. The results of these tests indicate that hot gases may be obtained in this manner for turbine drive applications. The temperature of these gases is not strongly affected by chamber pressure (throttling ratio). The data indicates that the combination of geometric parameters which results in the desired gas temperature (approximately 1500F) does not measureably affect injector performance.

TABLE II

TAPOFF TEST RESULTS

Gap, inches	Recess, inches	Chamber Pressure, psia	Gas Temperature, F	Tapoff Flow, percent
0.006	0.20	423	-	-
0.006	0.30	411	1600*	1.1
0.009	0.30	290	1020	1.2
0.009	0.30	353	940	1.1
0.009	0.30	483	1030	1.4
0.012	0.30	274	335	1.4
0.012	0.30	468	400	1.5

* Extrapolated

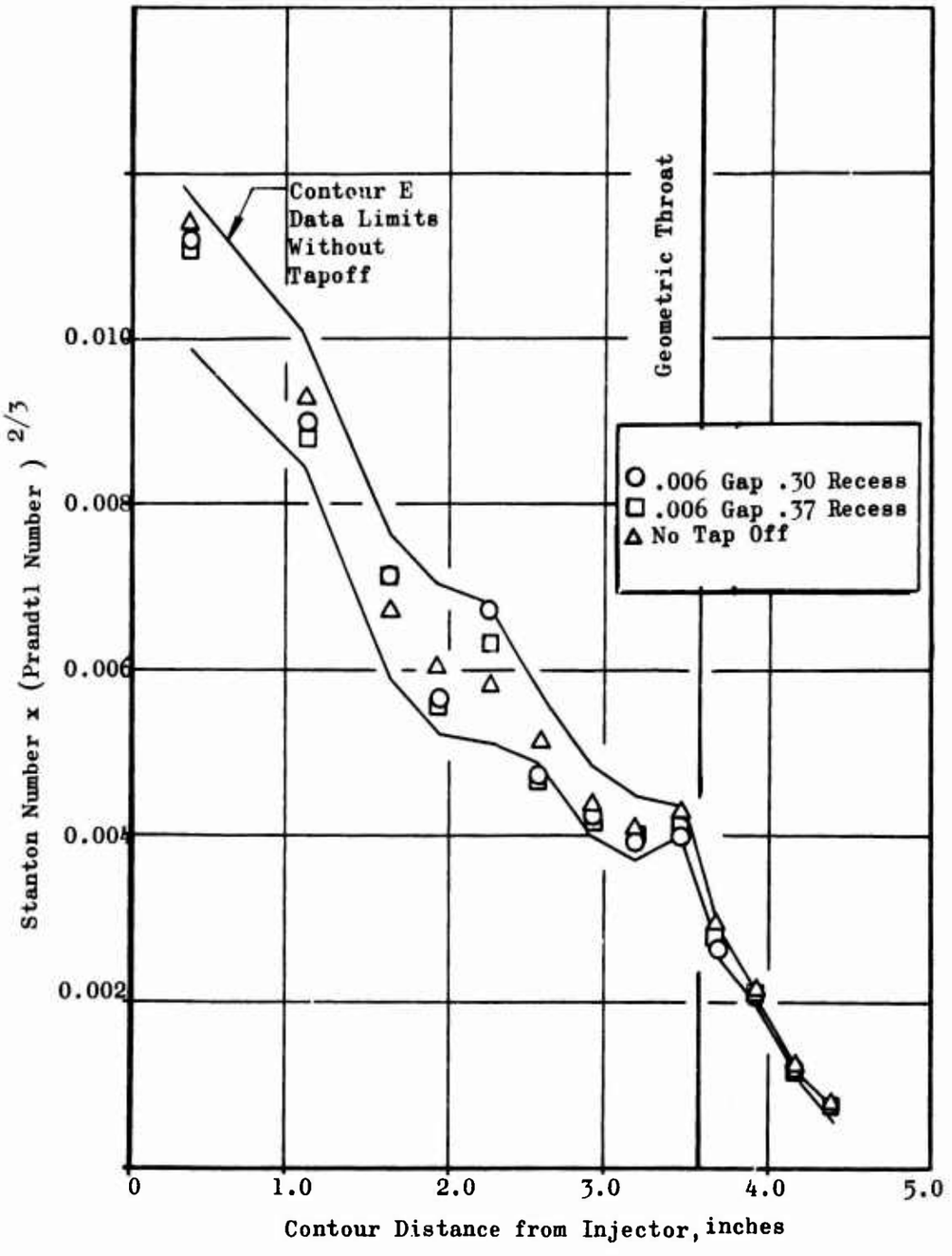

Figure 5. Effect of Tapoff on Heat Transfer
Contour E

2. MIXTURE RATIO BIAS AND OTHER TESTS

(U) Tests to determine the effects of injecting small amounts of GH_2 at the edges of the injector along the combustion chamber contour walls were described in Ref. 3 . The objective was to conduct these tests with a nominal total injector mixture ratio. A final test was made during the report period with the special injector/chamber adapter shown in Fig. 6 . This adapter permits independent control of the GH_2 flowrates to the injector (core) and to the bias orifices.

(C) The test was conducted using a standard triplet injector in a Contour E chamber. The hydrogen bias flowrate was approximately 30 percent of the total hydrogen flowrate. The overall injector mixture ratio on this test (14.4) was higher than the nominal value so that the resulting mixture ratio of the core was 20.6. The high-bias flowrate and consequent off-design operation of the core elements resulted in a performance degradation of 9 percent. Data from the previous tests indicate performance reductions of 8 percent for 12-percent mixture ratio bias.

(C) Redesign of the core for higher mixture ratio operation would result in substantially reducing this performance loss. However, the effect of mixture ratio bias on the heat transfer rates appears to be small. The heat transfer data for this test and for the previous mixture ratio bias tests with Contour E are shown in Fig. 7 for the nozzle portion of the chamber. A reduction of the heat transfer rate by approximately 20 percent is indicated. The reduction does not appear to be proportional to the bias flowrate;

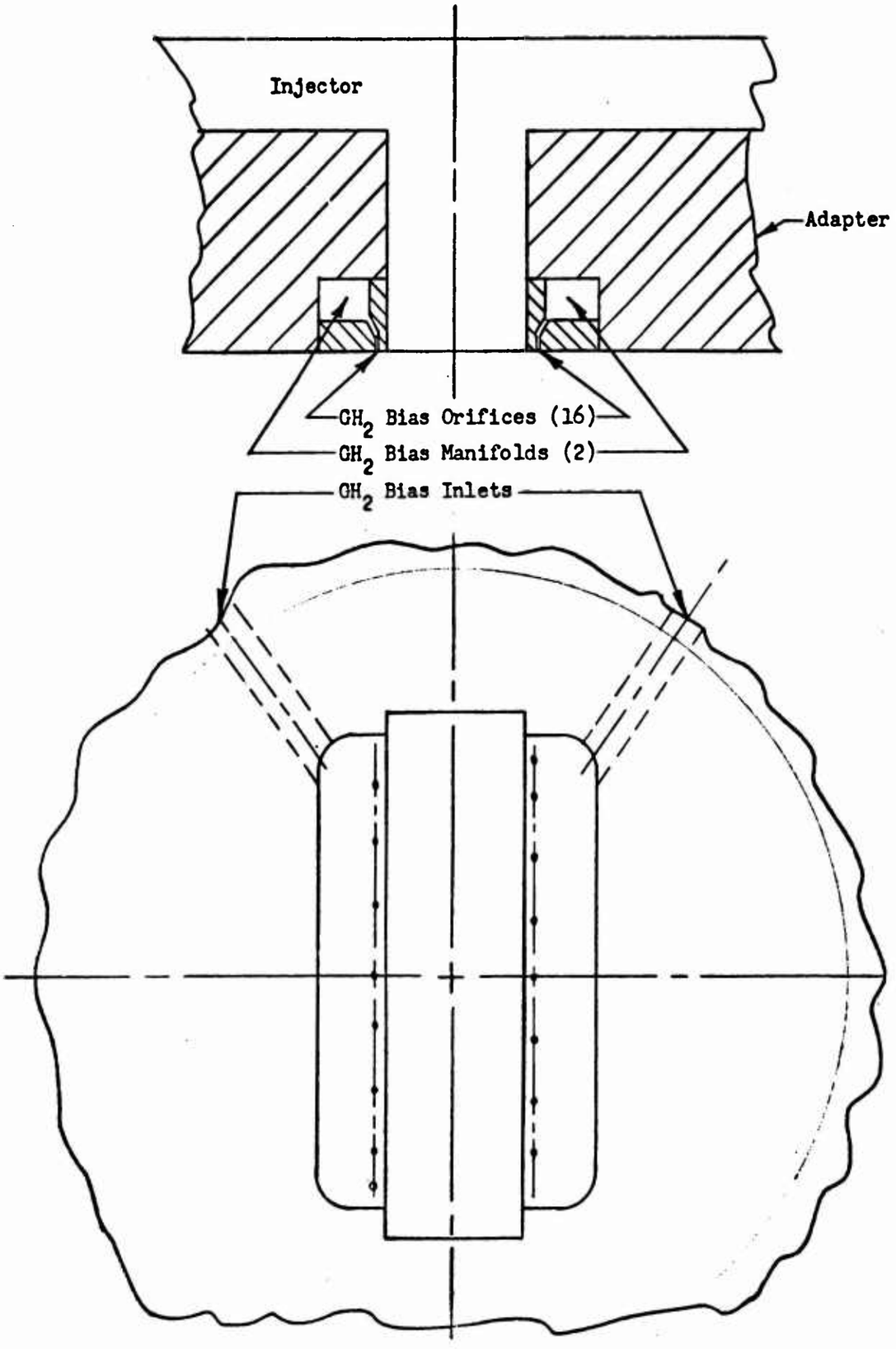

Figure 6 . Adapter for Mixture Ratio Bias

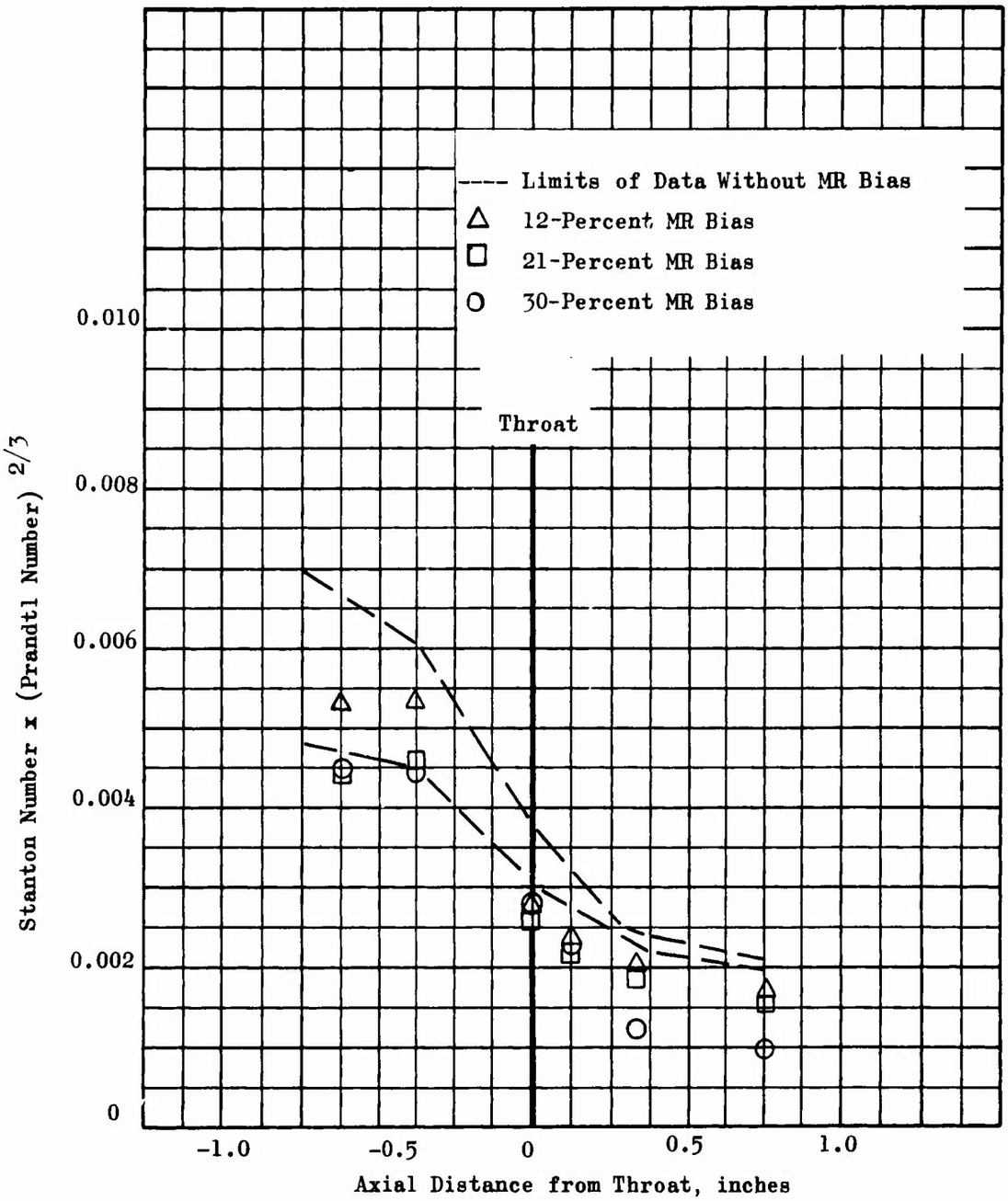

Figure 7. Effect of Mixture Ratio Bias on Nozzle Heat Transfer Parameter - Contour E.

the reduction with 30-percent bias flow appears to be similar to that with 12-percent GH_2 bias. The throat data values for the three tests probably represent nearly the same actual value within the limits of repeatability. Use of the Stanton-Prandtl parameter is made to desensitize the heat transfer coefficient values to such influences as chamber pressure and mixture ratio variations as discussed in Ref. 3 .

(C) A number of combustion chamber geometries and injector configurations have been fabricated and tested under company-sponsored programs. The results of these tests indicated that a marked reduction in heat transfer rates in the combustion zone and throat regions could be obtained while maintaining the potential for high performance. The injector/combustion chamber contour which provided such results was an impinging fan injector in a combustion chamber which converged continuously from the injector to the throat at a 15-degree angle. The injector elements are formed by two pairs of LF_2 orifices forming two fans which intersect above three axial hydrogen orifices. A triplet-element injector was also fabricated and tested with this contour but did not perform as well as the impinging fan injector.

(C) A series of tests were conducted with the Contour E chamber and the triplet injector with GH_2 orifices enlarged to 0.055 inches as part of the injector characterization tests (Ref.3). The nominal injector GH_2 orifice diameter is 0.037 inches and demonstrates 97 percent η_{c^*} performance. The injector with enlarged orifices indicates a slight performance decrease with respect to the nominal injector. The impinging fan injector with one row of elements was tested during the report period. The simplicity of fabrication of this injector led to its construction even though it was evident that some performance degradation was possible because of the concentration of elements on the centerline of the injector face. Data from other test programs demonstrate that with similar element location and orientation the impinging fan type injector yields performance superior to that of the triplet injector.

SECTION IV

TASK III - TUBE-WALL SEGMENT EVALUATION

(U) The tube-wall segment evaluation task encompasses three areas: (1) nozzle throat inserts, (2) complete tube-wall segments; and (3) structural segments. The results of the Task II effort (solid-wall segment evaluation) provide design data for each of these areas.

(U) The contour-evaluation data are used to specify the internal dimensions of the Task III hardware. The optimum injector configuration, determined from solid-wall chamber tests, is used with the tube-wall throat inserts and the tube-wall segements. The heat transfer data obtained with the solid-wall hardware specifies the coolant velocities and number of passes required for the tube-wall configurations.

1. TUBE-WALL THROAT INSERTS

(U) The tube-wall throat insert represents an intermediate step between the solid-wall and tube-wall segments. The purpose of the inserts is to provide a relatively inexpensive means of verifying the tube-wall design in the most critical area, the throat region.

(U) The drawing of the tube-wall throat insert is shown in Fig. 8 . The nozzle contour is the same as that of the solid-wall segment. One side of the nozzle contour is water cooled in a manner similar to the solid-wall segment nozzle. This permits determination of the thermal environment to which the tube-wall is exposed. The side walls of the insert are also water cooled.

(U) The other contour side of the throat insert is formed by a bank of constant cross-section hydrogen-cooled tubes. The cross-sectional dimensions of the tubes are representative of the dimensions at the throat of a tube-wall segment.

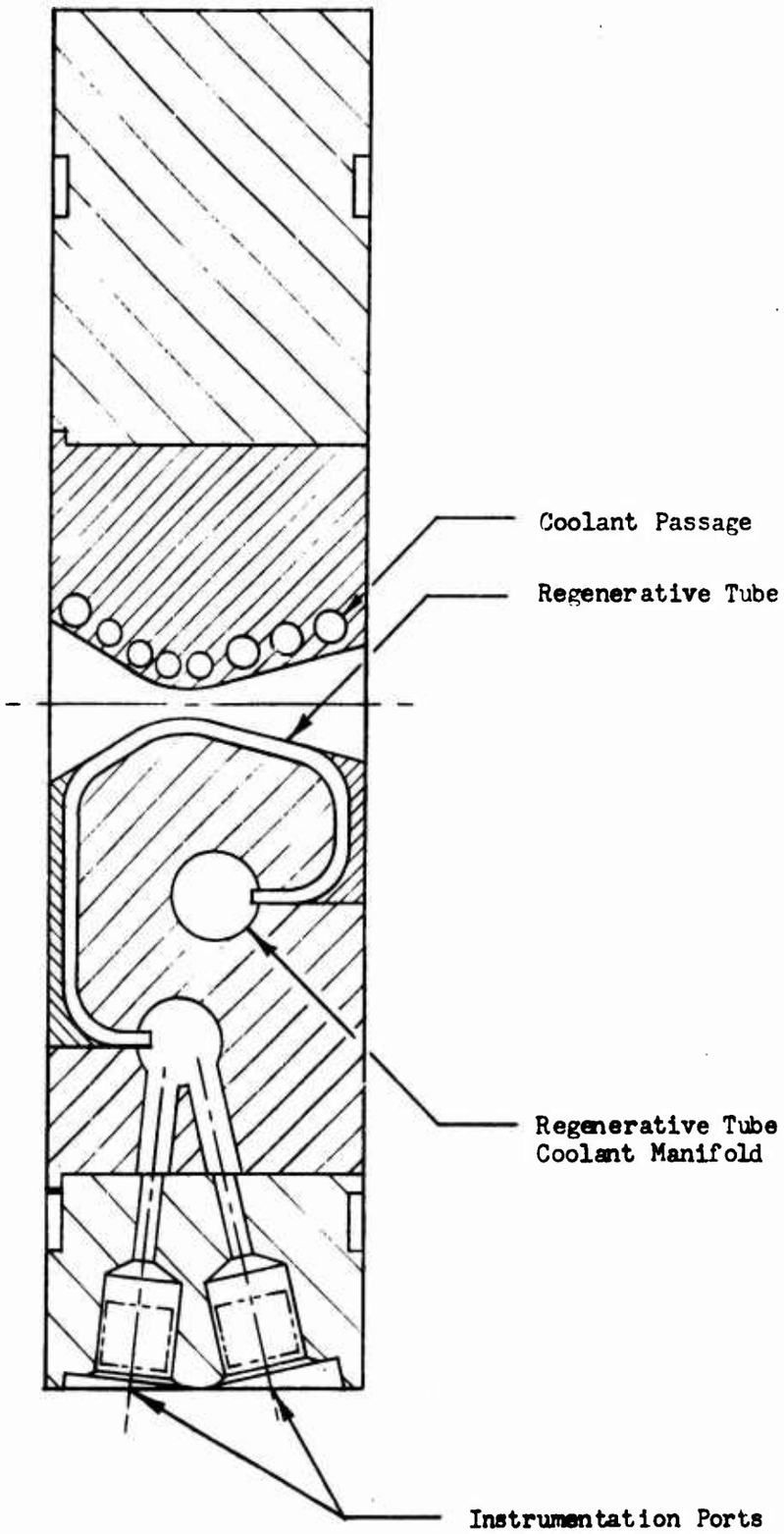

Figure 8. Tube-Wall Throat Insert

(C) The difference between the two inserts being built is the tube material and dimensions. One insert uses nickel tubing, while the other insert uses CRES tubing. The hydrogen manifolds are each instrumented for temperature and pressure measurements (only one set of instrumentation taps is visible in Fig. 8). The combustion chamber and nozzle insert assembled for testing are shown in Fig. 9.

(U) For very low hydrogen temperatures, the effect of hydrogen temperature on heat transfer rates is quite significant. Therefore, to simulate the first-pass flow conditions, the liquid hydrogen must be heated prior to entering the insert. The amount of preheating depends upon the degree of heating expected in the combustion zone of the chamber, since the tubes only include the converging portion of the nozzle near the throat. To simulate a range of preheating conditions, the test facility was provided with the features shown in Fig. 10. Both liquid and gaseous hydrogen are provided and combined in a mixing chamber when very low-temperature hydrogen is required. The use of a LN_2 heat exchanger in the gaseous hydrogen line was found to be a more satisfactory method of providing hydrogen at temperatures above 200R. The hydrogen flowrate for this latter configuration is measured accurately by a sonic venturi prior to chilling in the heat exchanger. The same venturi is used to measure the flowrate of the GH_2 when it is mixed with LH_2 in the mixing chamber. This GH_2 flowrate measurement is added to the LH_2 flowrate measured by the turbine flowmeter to obtain the total hydrogen flow.

a. Nickel Tube Insert

(C) Fabrication of both tube-wall inserts was completed during the report period. The nickel tube-wall insert is shown in Fig. 11. The large inlet tubes are the hydrogen-coolant manifold inlets; the smaller tubes

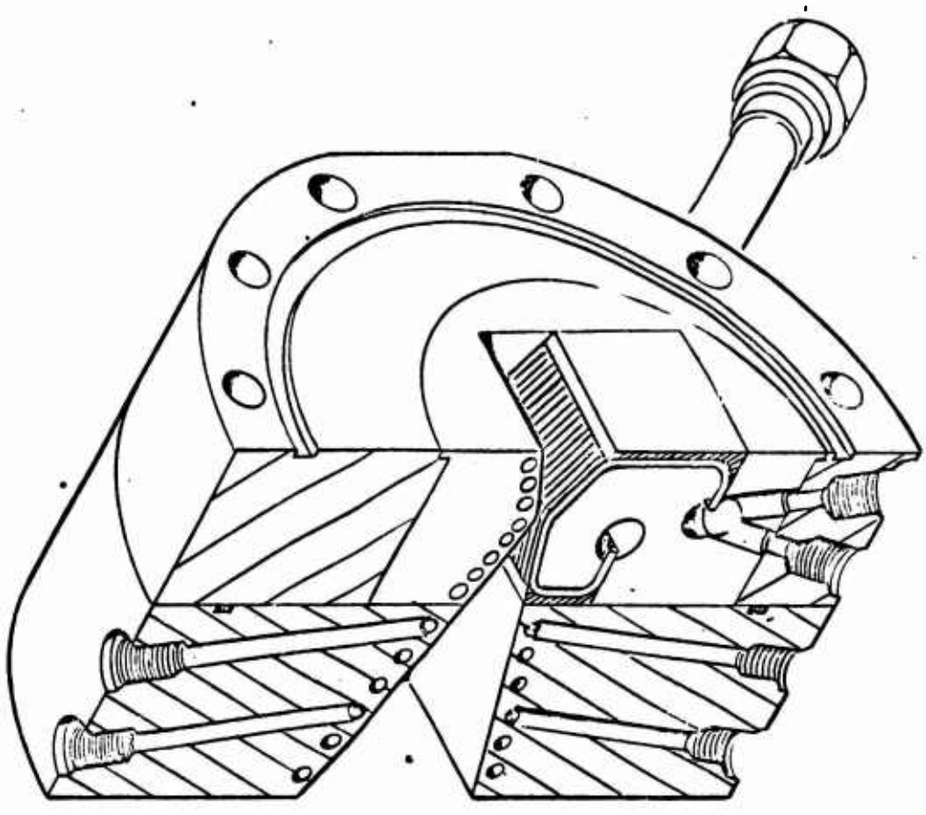

Figure 9. Tube-Wall Insert and Water-Cooled Chamber

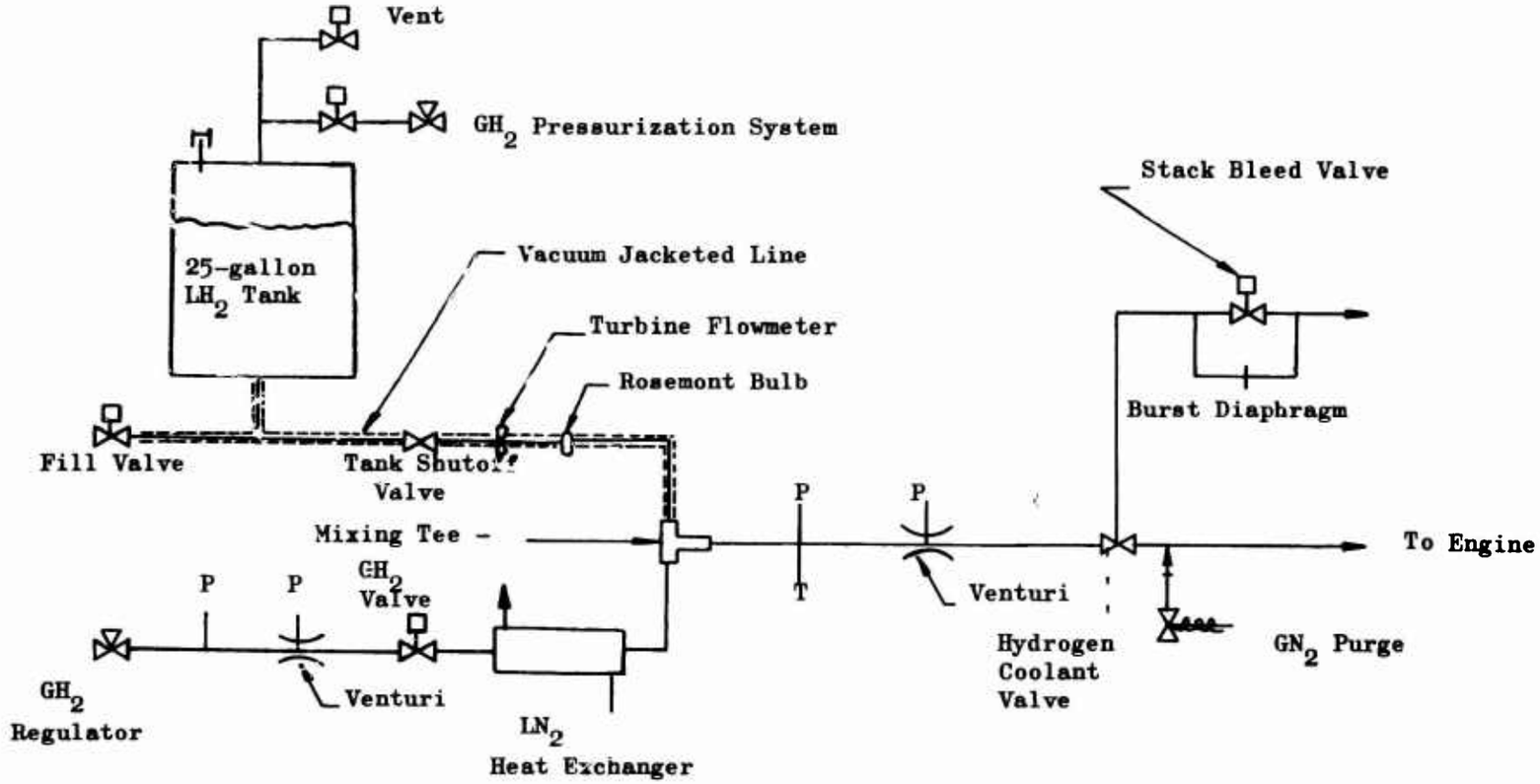

Figure 10 . Facility Schematic Showing Regenerative Cooling Lines

are the inlet and outlet tubes for the water-cooling passages. The nickel insert was completed first and sent to the test facility for water-flow calibrations of the water-coolant passages and the hydrogen-cooled tubes prior to hot firing tests. Abnormally high pressure drops were noted in the hydrogen tubes and the insert was returned for further examination.

(C) A single nickel tube was formed to the shape of those in the tube bundle and brazed to an inlet manifold. The measured single-tube water flowrate of 0.039 lb/sec at 100 psi ΔP agreed fairly well with the analytically predicted value at 0.034 lb/sec. The ends of the tubes at the insert entrance and exit manifolds were inspected with borescopes and found to be clean and free of obstruction. A hole bored through the face of the insert permitted further inspection of the tube ends and confirmation that no restrictions were present at this location. Wires used to probe the tubes through the exposed tube ends located some partial and some complete blockages. Each tube had been subjected to a semiquantitative flow check after brazing to the backup structure, so that it is improbable that the restrictions occurred prior to this time in the fabrication process. Subsequent fabrication operations on the insert consisted of brazing the face plates and sideplates to the hydrogen and water-cooled contour walls, silver plating the circumference of the core after machining to a round surface, eutectic bonding of the core to collar, and installation to the hydrogen and water inlet and outlet tubes. Partial assemblies of these components are shown in Ref. 3.

(U) A sample of a crystalline substance was collected from the tubes and subjected to analysis by X-ray diffraction techniques. The results of this analysis indicated that the material in the tube was primarily (SiO_2)

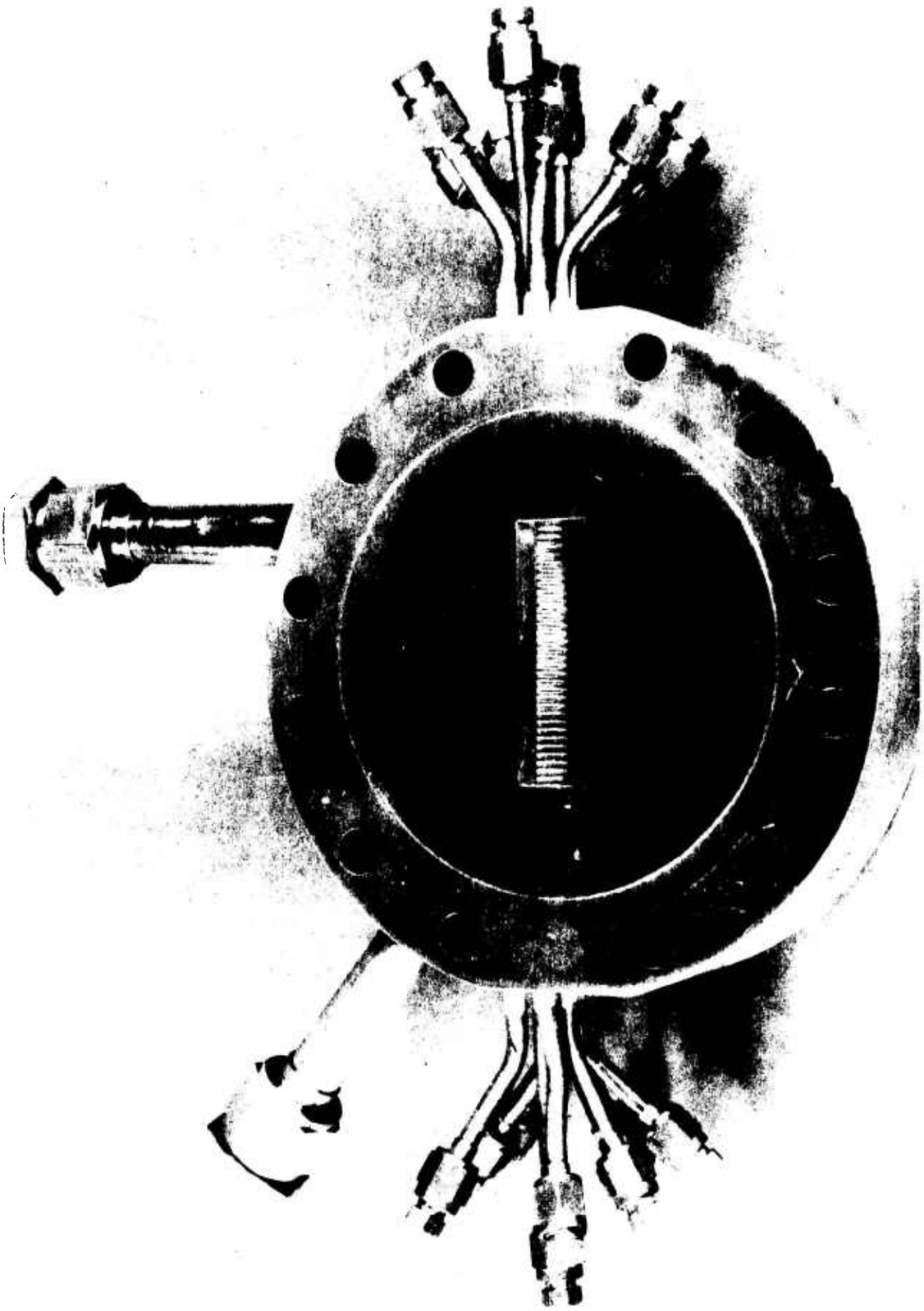

Figure 11 . Nickel Tube-Wall Throat Insert

silicon dioxide. Methods of removing and determining the source of the material are being investigated.

b. CRES Tube-Wall Throat Insert

(C) The CRES tube-wall throat insert was completed shortly after the nickel tube insert. A water-flow check of the CRES insert was performed, and the pressure drop vs flow data agreed fairly well with the predicted values. As shown in Fig. 12, the measured pressure drops were lower than the estimated values.

(C) A short-duration (0.5 seconds) checkout test was first conducted at a chamber pressure of approximately 300 psia using ambient temperature GH_2 for the tube-wall coolant. A longer duration test was then conducted under the same conditions. The hydrogen mass flowrate for these tests corresponded to the injector hydrogen flow at nominal chamber pressure for a two-pass flow system. Inspection of the insert after this test revealed a leaking tube near one of the sidewalls.

(C) Two tests were then conducted with the same hydrogen coolant temperature and flowrate. The chamber pressures during these two tests were 300 and 504 psia. The predicted maximum tube-wall temperature at the throat of the nozzle based upon recently obtained solid-wall segment test data is shown in Fig. 13. The method of calculating the gas-side tube-wall temperature is outlined in Appendix B. No additional tube damage was visible after these tests.

(U) Test data indicated a high pressure drop across the fluorine injector orifices during the latter two tests. Heat transfer rates measured on the water-cooled side were slightly higher than those measured previously in completely water-cooled hardware, and the performance was slightly lower. A plugged injector was suspected. This was confirmed by a water-flow check

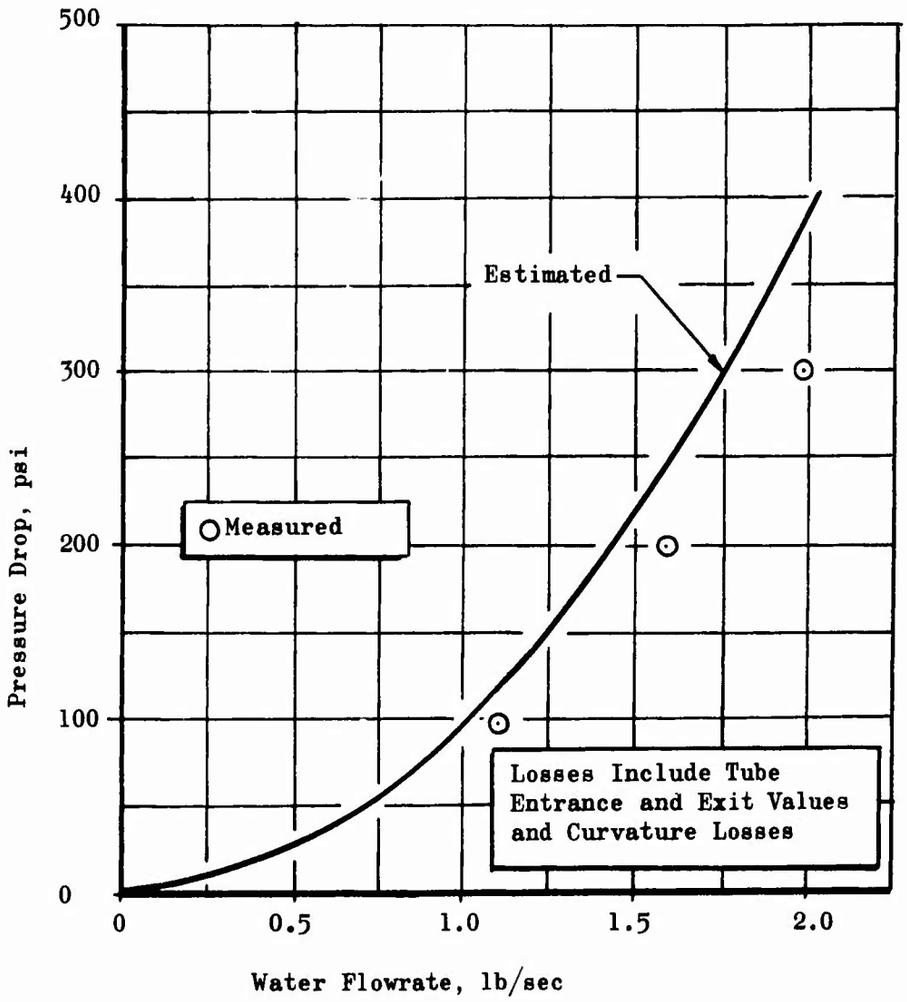

Figure 12 . Estimated and Measured Pressure Drops for Water-Flow Calibration of the CRES Tube Throat Insert

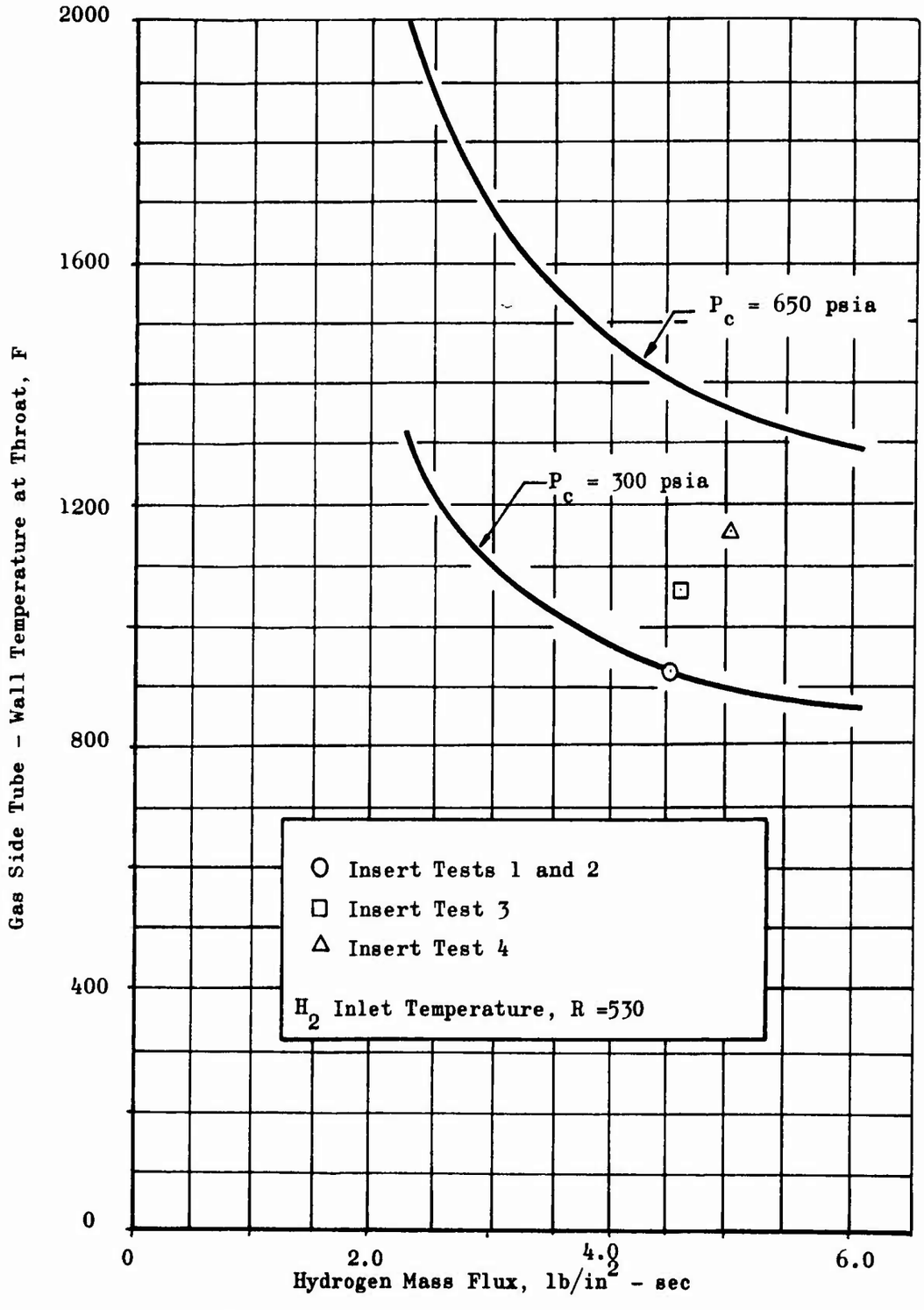

Figure 13 . Design Tube - Wall Temperature vs Hydrogen Flow for the CRES Tube Insert

which showed misimpingement between several orifices. The injector was cleaned and was again water flowed to ensure proper impingement of the oxidizer streams.

(C) The fifth test of the CRES tube insert was conducted at a chamber pressure of 642 psia with chilled hydrogen as the coolant. Conditions for this test and the preceeding ones are detailed in Table III. Fourteen of the tubes were found to be eroded after the test. Preliminary analysis of the data indicates a chamber pressure overshoot was responsible for the tube damage. Motion pictures of the test and other test data indicate that the failure occurred early in the test. The chamber pressure rose to 835 psia, an excessive value for this design, during the start, and maintained this pressure for a sufficient duration for the 0.012-inch thick CRES tube walls to reach thermal equilibrium. A detailed analysis of the test data is continuing and will include an examination of the sectioned tubes of the insert.

(C) The tube sectioning thus far has indicated that the tube which failed during the low ($\sim$ 300 psia) chamber pressure test had a plug of braze material at the entrance. Since all tubes were individually flow checked prior to assembling the side plates to the strongback, it is concluded that the plugging occurred during this braze operation. The possibility of this happening on the tube wall segments has been eliminated by welding a plug over the manifold ends prior to brazing in the sideplates.

2. TUBE WALL SEGMENTS

(C) The purpose of the tube-wall segment is to demonstrate complete regenerative cooling capability for the thrust chamber. Two identical units are being fabricated using constant outside diameter nickel tubes. A tube

TABLE III

SUMMARY OF STAINLESS STEEL TUBE INSERT TESTS

Test	Duration (Seconds)	Nominal Chamber Pressure (psia)	Mixture Ratio	Flowrate (lb_m/sec)	T_{inlet} (^oR)	T_{bulk} (^oF)	P_{inlet} (psia)
1	0.5	300	-	-	-	-	-
2	3.5	291	12.6	0.225	532	72.5	1398
3	2.0	390	14.6	0.229	543	79	1490
4	2.0	504	14.2	0.248	547	83	1546
5	2.7	642	15.3	0.547	210	79	2168

CONFIDENTIAL

having variable inside diameter with constant outside diameter is formed from a constant cross-section tube by tapering the tube to the desired internal contour, plating the tube, and grinding the plated tube to the required OD. The segment design incorporates two-pass cooling of each contour wall with external ducting for crossover and injector feed after cooling. The side walls of the segments are independently water-cooled. A non-flightweight support structure consisting of copper strongbacks for the tube bundles and a steel collar is included. Structural integrity using lightweight structures is to be demonstrated in separate non-firing hardware.

(C) The tubes are electron beam welded together to form a continuous tube bundle and then formed to the shape of the contour as shown in the sample tube bundle depicted in Fig. 14. This assembly technique results in a more uniform tube bundle cross section, eliminates the possibility of braze washout between tubes, facilitates controling the tube cross section during the forming operation, and decreases the effort required to form and braze tubes to the strongback. A microphoto of electron beam welded tubes is shown in Fig. 15. An excellant bond formed by the parent material of the tubes is noted. A lightweight joint is formed because no additional weld material is used in the process. After determining the required equipment settings on the basis of a sample run, the weldor can be operated at a maximum speed of 50 inches per minute. The width of the weld and dept of penetration can be controlled over wide ranges. The welding is accomplished under vacuum conditions in a shielded chamber the dimensions of which establish the limits of the size of the component to be welded.

(C) Isometric and exploded views of the segment are shown in Figs. 16 and 17 respectively. The combustion chamber converges continuously to the throat at a 17-degree angle. This contour was selected on the basis

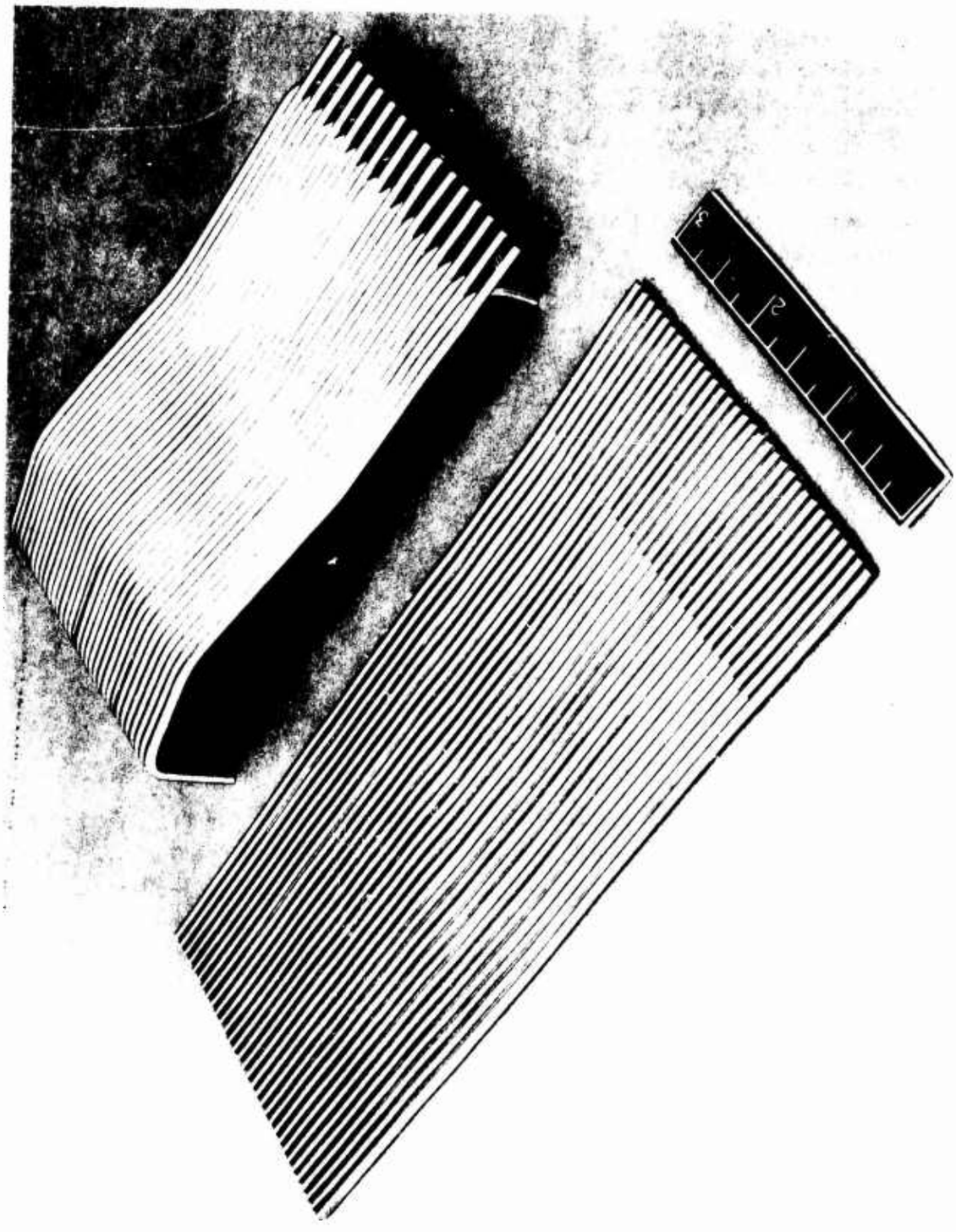

Figure 14 . Sample EB-Welded Tube Blankets
Before and After Forming

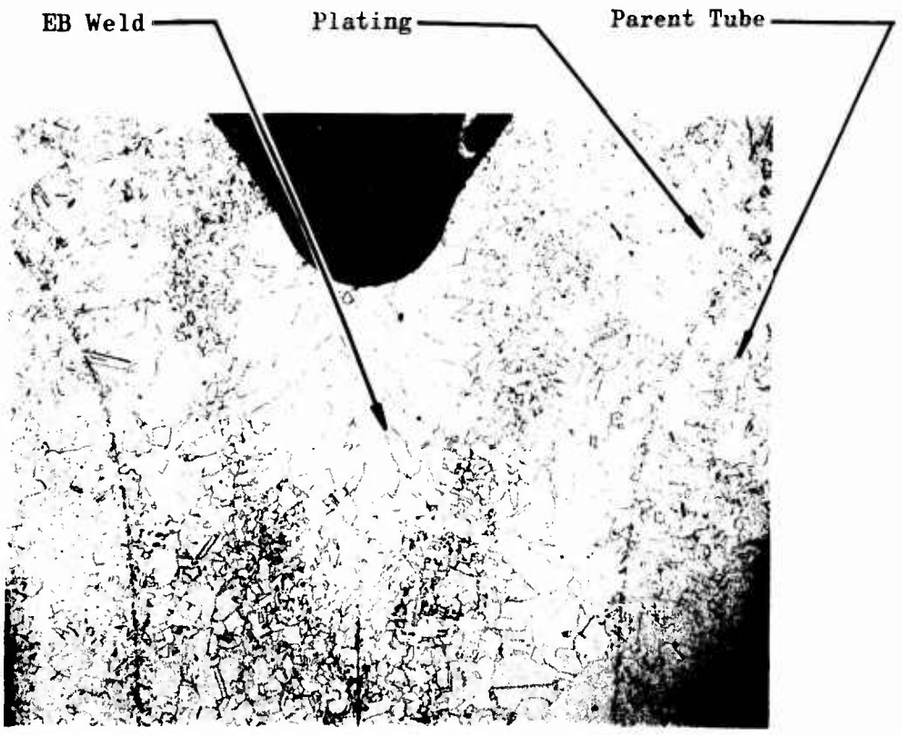

Figure 15. EB Welded Plated Nickel Tubes

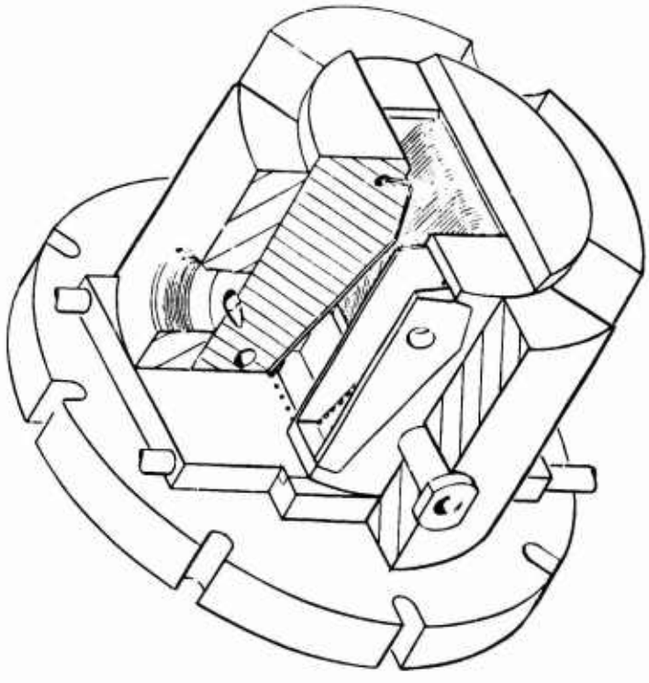

Figure 16. Segment, MSPS Tube Wall

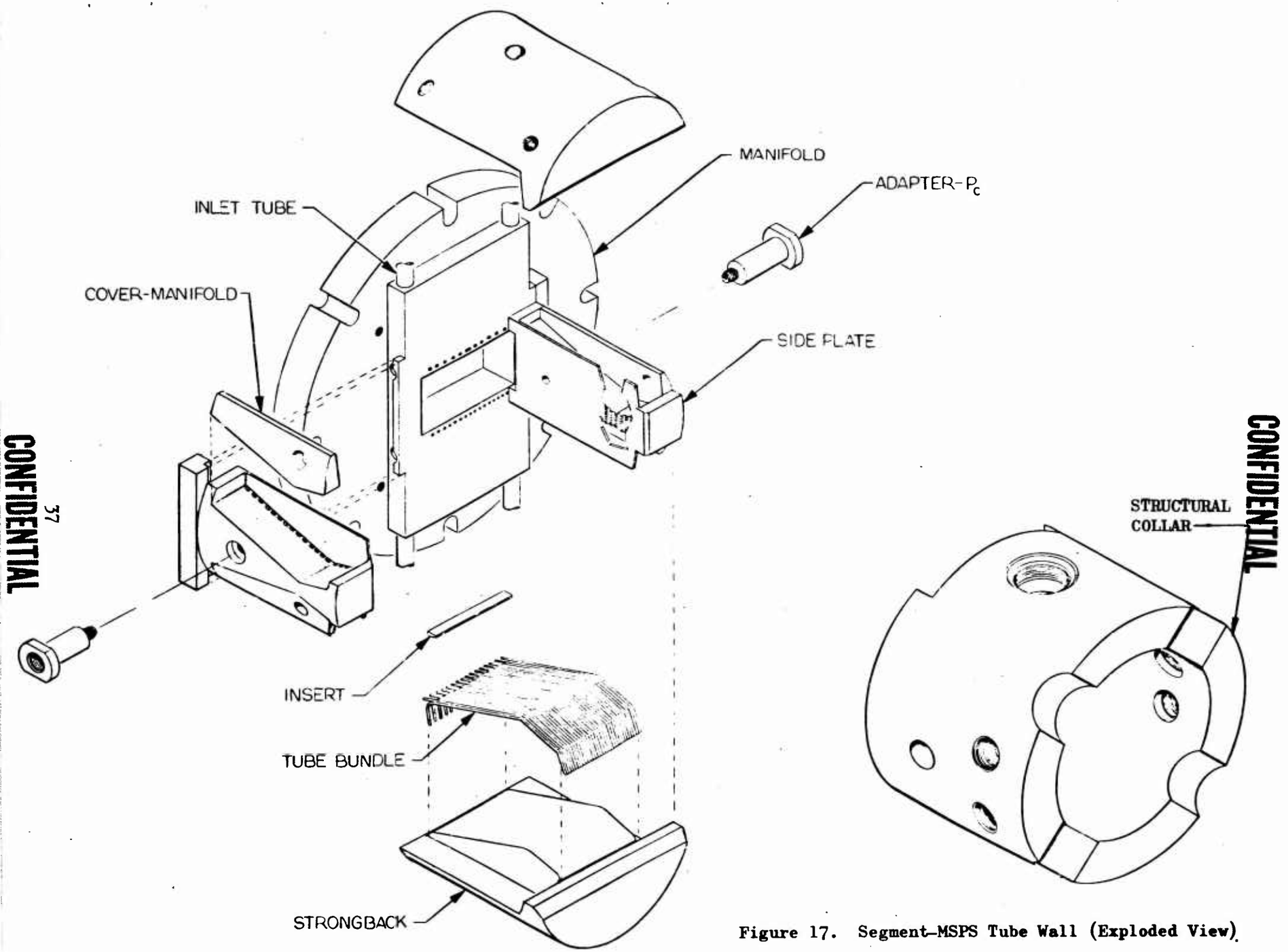

Figure 17. Segment-MSPS Tube Wall (Exploded View)

of results of tests of water-cooled segments on this program and on related program tests. These results indicated lower heat transfer rates in the combustion region and nozzle for this contour compared to the best of the previous contours, Contour E.

(C) Heat transfer analysis resulted in the specification of unequal numbers is tubes in the first and second passes on the first-cooled side of the chamber. Twelve first pass tubes are used compared to 20 second pass tubes because the warmer hydrogen in the second pass has better cooling properties and therefore requires a lower coolant mass velocity for a given tube wall temperature. Equal numbers of tubes are used in the first and second passes on the other side of the chamber because the coolant properties of the hydrogen are strongly sensitive to temperature only at low temperatures.

(C) All components for both segments have been fabricated except the tube bundles. Tubes were tapered for both segments. The tubes for the first segment were plated and ground to a constant outside diameter. Inspection of the tubes at this point indicated an unsatisfactory bond between the parent tube material and the plating. Since sample tubes had been previously plated by the same process the plating solutions were analyzed and impurities were found in one of the preplating solutions. In the course of the investigation it was determined that good bonds could be obtained when the particular preplating solution was eliminated. Another set of tubes has been drawn and plated by this method with samples being subjected to microscopic examination. A cross section of a tube plated in this manner and annealed is shown in Fig. 18 . The excellent bond can be seen by noting the actual growth of crystals across the barely visible interface between the tube and plating material.

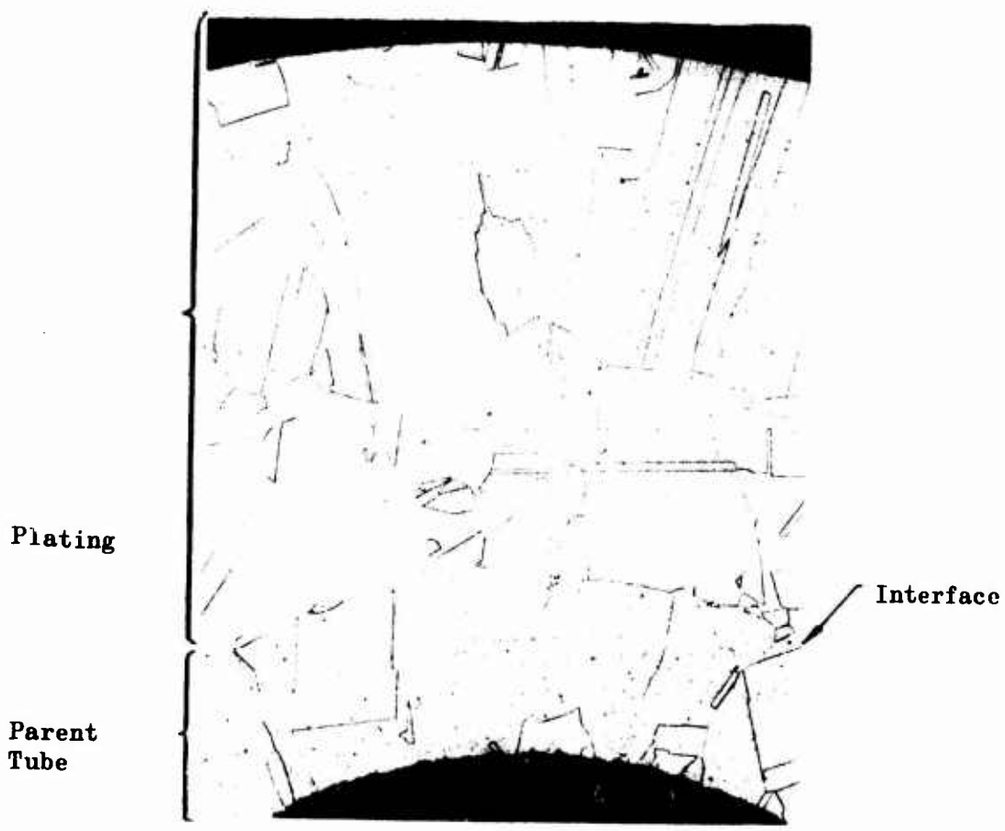

Figure 18. Cross Section of Nickel-Plated Tube

3. STRUCTURAL TEST SEGMENTS

(C) The purpose of the structural segments is to establish the effectiveness of rib and honeycomb support structures and to demonstrate, by means of mechanical loading tests, that the throat area can be maintained within 10 percent over the 9 to 1 throttling range. Designs and analysis for these segments have been completed and the results presented in the previous quarterly progress reports. Fabrication of both segments is in progress with the honeycomb segment scheduled for completion as soon as the structural testing of the rib segment has been completed. Both segments are nearly flightweight. Additional weight savings could be effected by the means suggested in Ref. 3 .

(C) The segments are identical except for the structural material used as a beam structure between the baffles. Each consists of three six inch compartments formed by the end plates and two structural baffles. The two outer compartments serve to isolate the center compartment from the effects of the end plates. The test conditions for the center compartment thus simulate very closely the chamber pressure induced forces acting on a compartment of a complete toroidal chamber. The walls of the chamber are bolted together and indexed by the baffles. It was tentatively planned to use hydraulic bladders to simulate chamber pressure in the segments. Recent tests have indicated that the use of metallic throat plugs with a thin rubber coating provide a more effective sealing method and closer simulation of chamber pressure.

a. Rib Segment

(C) An isometric drawing of the rib structural segment is shown in Fig.19 . The rib panels are formed by welding accurately formed rib channels together. An investigation of tungsten inert gas, TIG, and electron beam, EB, weld-

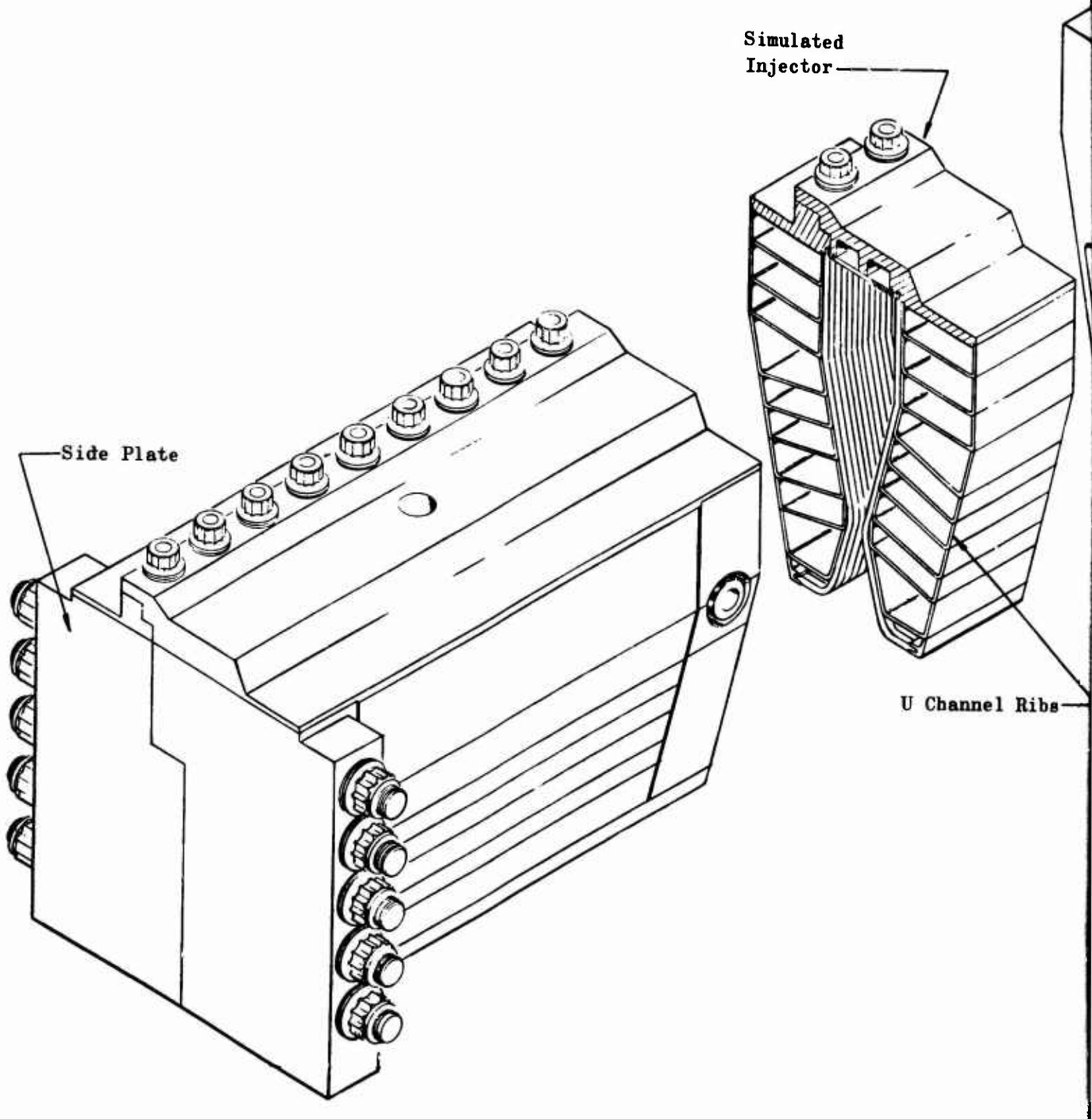
Simulated
Injector
Side Plate
U Channel Ribs

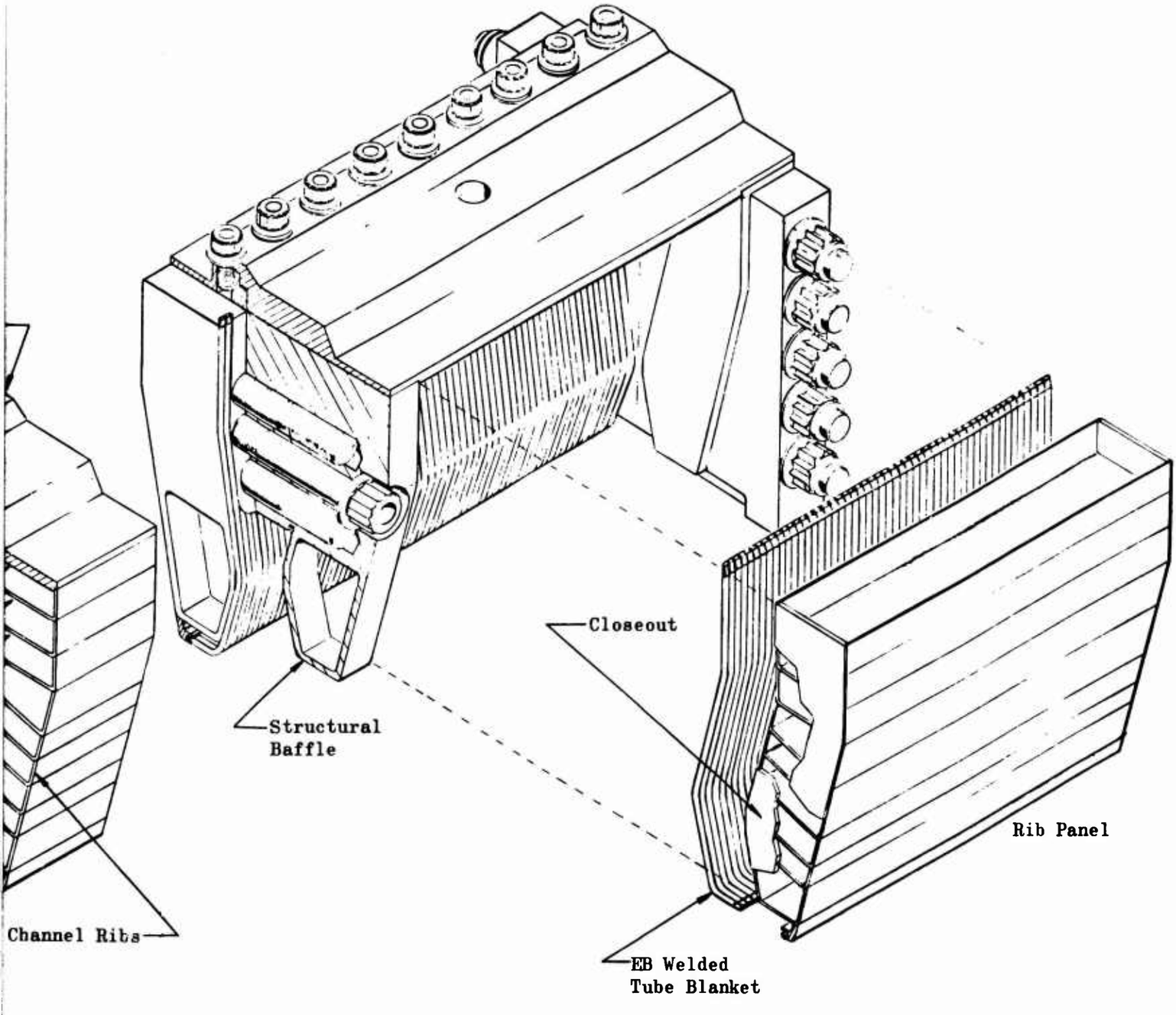

Figure 19. Rib Structure Segment

ing methods was conducted to determine the process most applicable to the rib structural segment. TIG welding has the advantage of requiring less exact fitting tolerances prior to welding since the weld rod metal can bridge small surface discontinuities. However, if proper fitting tolerances can be held, the EB welding technique results in a cleaner and lighter weld since the parent material supplies the molten weld material. The width and penetration depth of the weld are determined by control settings on the equipment. Once these proper settings have been determined by a sample weld, all channel welds are made at the same settings so that a uniform weld is rapidly made. Test samples of channels were EB welded to provide the optimum equipment settings and to determine if fitup problems did exist. The fitup designs and techniques proved to be quite compatible with the EB welding process and very good samples were obtained. A photograph of an EB weld sample and an enlargement of one of the channel to channel EB welds are shown in Fig. 20 .

(C) The beginning of the assembly is shown in Fig. 21 . The U channels are preformed, cut to length, and pierced with a venting hole. They are then assembled onto the milled closeouts which serve as jigs during assembly and structural reinforcing members thereafter. A complete panel, fitted into the closeouts is shown in Fig.22 . The tapped holes in the closeouts are used in bolting the assembly into the weld fixture which prevents distoration of the panel during the welding operation. The completely welded panel is shown in Fig. 23 . The milled slots in the closeouts provide locations for butt welding the panels to the closeout. The closeouts will be milled down, removing most of the material visible in the photographs and leaving only sufficient material for welding to the structural baffles. A closeup

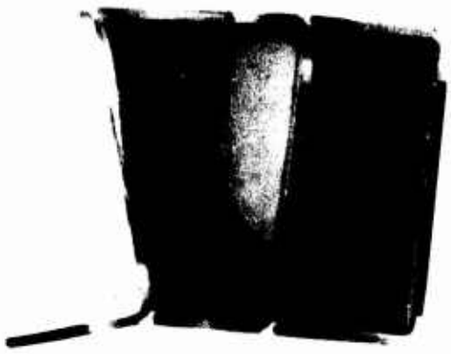

a. EB Welded Channels

b. EB Weld Closeup

Figure 20. Rib Channel EB Weld Sample

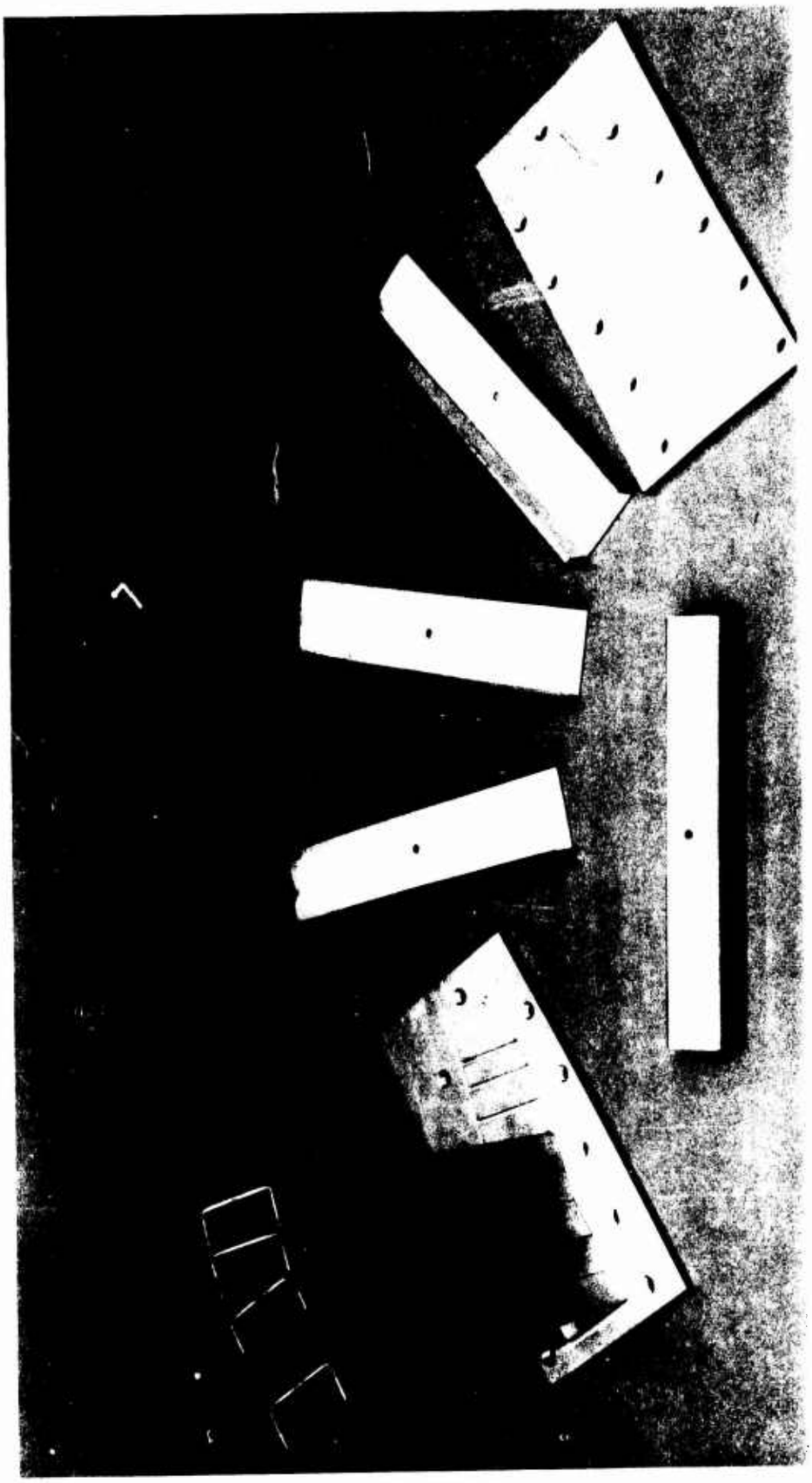

Figure 21 . Partial Assembly of Rib Panel

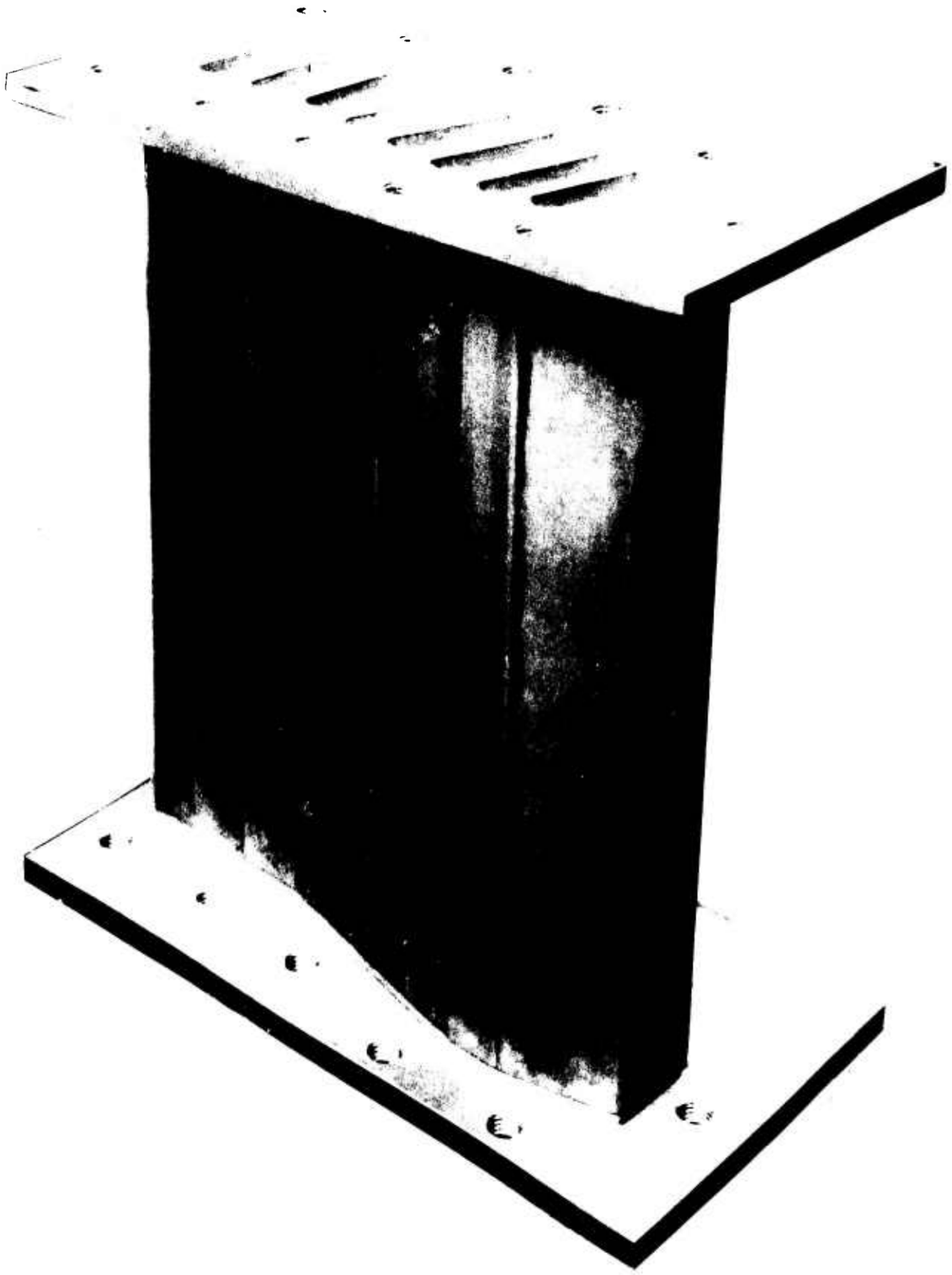

Figure 22. Rib Panel Before Welding

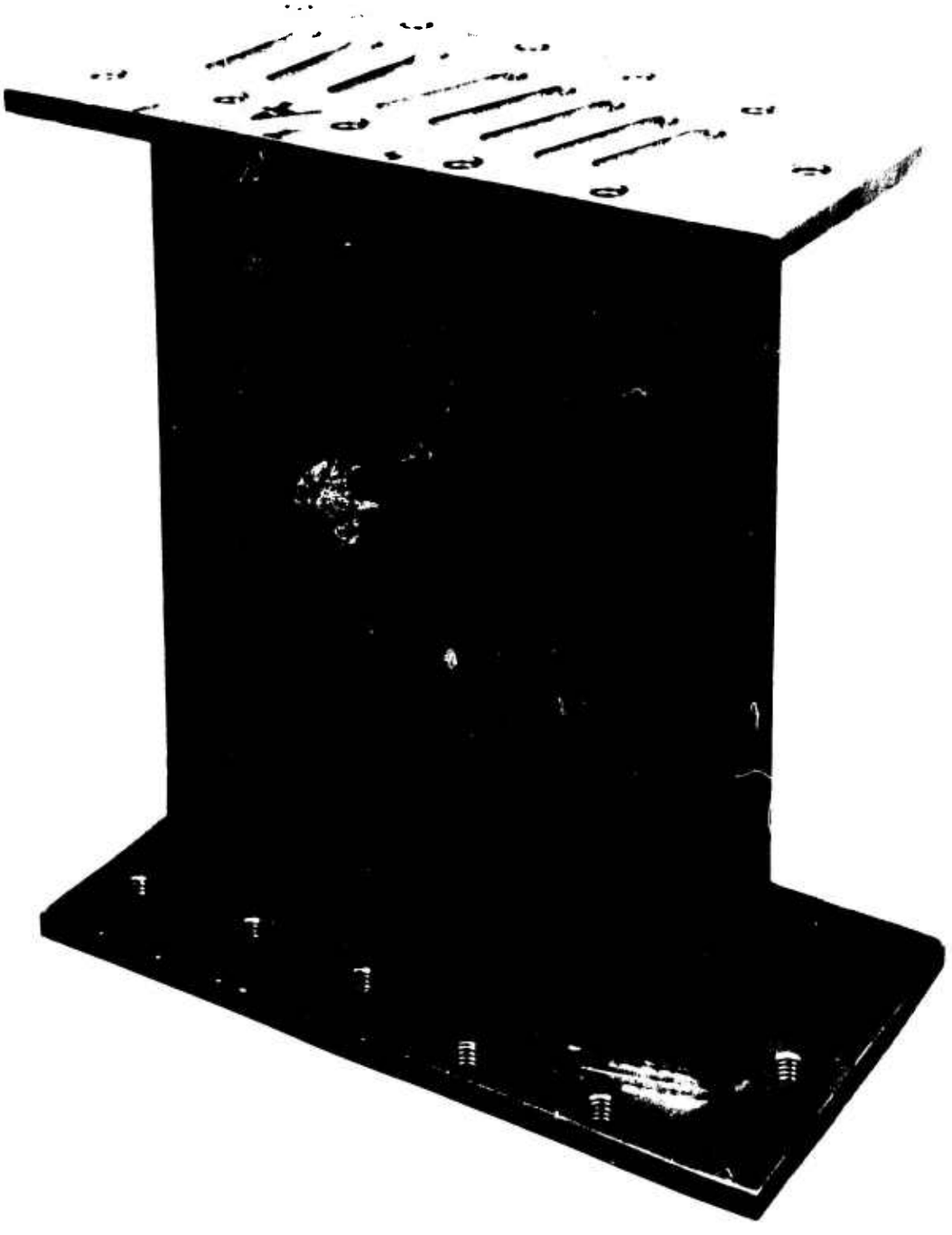

Figure 23 . Rib Panel After EB Welding

view of the EB welded channels and closeout is shown in Fig.24 . The uniformity of the weld is evident in this photograph. The lines between the channel welds are scribe marks used for location purposes.

b. Honeycomb Segment

(U) Originally it was planned to fabricate a complete honeycomb structural segment which differs from the rib segment only in the panel core material used to provide rigidity and to transmit the chamber pressure induced loads to the structural baffles and injector. Recent analyses, outlined below, resulted in the conclusion that accurate throat gap variations for a complete honeycomb segment could be obtained by doubling the deflections measured on the honeycomb wall side of a composite segment consisting of one honeycomb side and one rib side. To reduce fabrication time and effort, therefore, only one honeycomb side (the outer wall) is being fabricated in addition to the complete rib structural segment.

(U) Two factors were determined by the analysis: (1) the equality of deflection of the inner and outer walls was established to verify the procedure of obtaining the throat gap variations by doubling the honeycomb wall deflections; (2) the effect of the moment of inertia of the inner wall on the deflections of the honeycomb outer wall.

(U) The inner and outer bodies are mirror images of each other and differ only in that the inner body is welded to the baffles whereas the outer body is bolted to the baffles. The three outer wall-to-baffle bolts are pretorqued to values which prevent separation of the outer wall from the baffle. Under this condition the bolted and welded joints are identical with respect to the effect of throat gap deflections. Therefore, the inner and outer walls of a complete honeycomb segment would be expected to deflect equally.

Figure 24. Rib Panel EB Welds

(U) The effects of the inner wall rigidity on outer wall deflections were analyzed by isolation of the outer wall as a free body and consideration of the forces acting on it. Forces and moments result at the following locations:

a) chamber walls
b) baffle bolts
c) injector bolts
d) baffle bearing area
e) injector bearing area

(U) The direct effects of chamber pressure on each of the walls is independent of the other wall since the system is in static equilibrium. Injector bolt loads are independent of the inner structural panel design. Differences in moment of inertia between the rib and honeycomb structural panels could cause approximately a 3% difference in baffle bolt preload. The effect of this load differential will be localized to the baffle-bolt preload area.

(U) The forces and moments transmitted to the honeycomb wall by the injector and baffles depend upon the amount that these members deflect under the loads that are transmitted to them by either direct pressure or by the inner wall. If honeycomb and rib structural panels are considered as fixed end beams between baffles, the shear, S, and moment, M, transmitted to the fixed ends of such a beam of area A is dependent only on the pressure loading, P, as indicated by the equations

$$S = PA/2$$
$$M = PAL^2/12$$

The construction of the inner wall would, therefore, not affect the loads transmitted by the baffles to the honeycomb outer wall.

(U) Changing the inner wall from a honeycomb structure to a rib structure would affect the moment transmitted through the injector to the outer

honeycomb wall by an amount estimated to be less than 10 percent. This would, in turn, influence the throat deflection of the honeycomb wall by less than 1.5 percent. Thus, if a deflection of five percent of the initial throat gap would have occurred on each wall of a complete honeycomb segment, the deflection calculated by doubling the deflection of the honeycomb wall in the composite structure would be less than 5.08 percent. This difference, 0.08 percent or 0.0001 inches, is below the accuracy of the dial gauge instrumentation. Based on the above analytical results it was concluded that by measuring the deflections of the honeycomb side of a composite structural segment the data could be used to predict the deflection and throat area changes of a complete honeycomb segment.

(1) (C) Honeycomb Fabrication Samples. Samples simulating various facets of the honeycomb structural panel design were prepared before fabrication of the segment panels was initiated. The purpose of these samples was to ensure experience in all fabrication process details prior to making the actual honeycomb panels. The samples included a mechanical test specimen, a sample of nickel plating into honeycomb edge-like notches, subscale braze samples and a full-scale structural panel similar to those to be used in the honeycomb segment.

(C) The honeycomb structural panel design requires electroplating and machining operations to provide a flat surface of electroformed nickel on the irregular surfaces of three edges of a honeycomb core section while masking the two faces and the fourth edge. The honeycomb core is brazed to the face sheets to form a beam structure. A braze material had to be selected which has high strength at the elevated temperatures of the thrust chamber tubes carrying the regeneratively heated hydrogen to the injector. The nickel-plated layer at the edge of the core must

be electron-beam welded to inconel 718 baffles and injector. This weld must be of sufficient strength to transmit shear loads between the core sections and the baffles.

(U) Accordingly, the first fabrication sample involved nickel plating an inconel 718 block with notches machined along one edge to simulate the edge of honeycomb core. It was found that the nickel deposited more rapidly on the raised points of the edges and would tend, eventually, to form inclusions of plating solution. This tendency was eliminated by an initial plating operation, a machine cut across the edge to gain a flatter surface, and a final plating and machining of the surface (Fig. 25).

(U) The plated block was incorporated into a mechanical test specimen designed to establish the shear strength of the electron-beam weld between inconel 718 and the plated nickel layer. The nickel plated inconel 718 inner block was welded between the arms of a U-shaped outer block, also of inconel 718 as shown in Fig. 26 .

(U) Four welds were made between the plating layer and the U-shaped block, along top and bottom of the two opposite unnotched sides of the rectangular block. The notched plating specimen edge (simulating the exterior cells of the honeycomb panel) was oriented prependicular to the welded edges so that failure of the welds would not distort the plating over the notches. Weld penetration was sized so that the specimen would fail in shear across the welds. As the weld beads were essentially castings of molten inconel 718 plus pure nickel, it was expected that the weld shear strength would be intermediate between that of pure annealed nickel and that of inconel 718, a nickel base alloy.

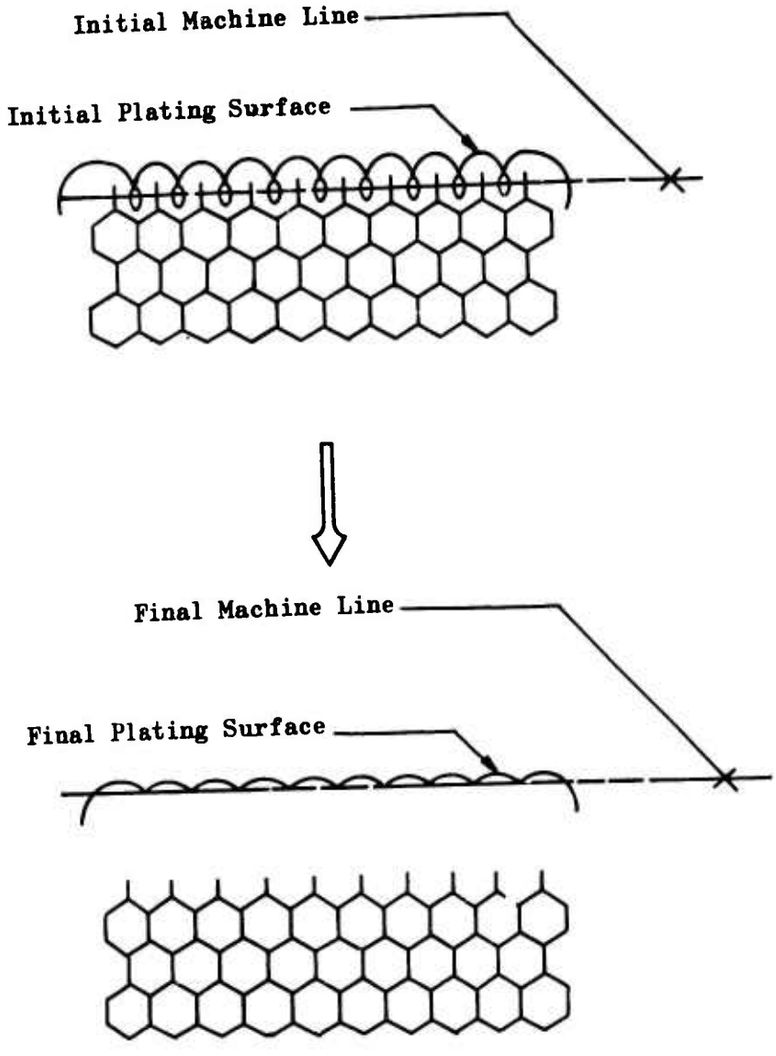

Figure 25 . Honeycomb Edge Plating Sample

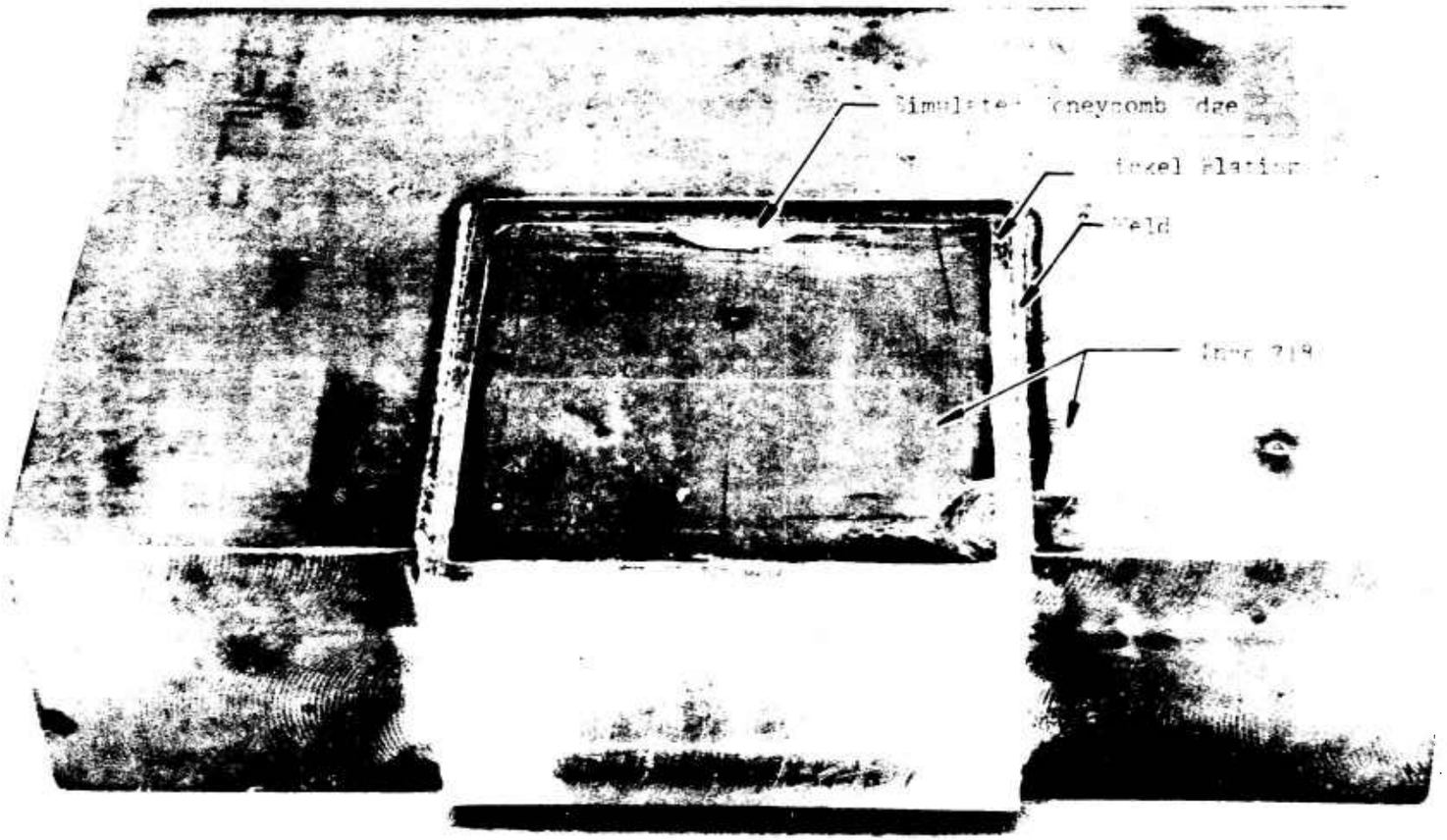

Figure 26. Nickel Plating and Weld Sample

(U) The specimen was heat treated after weld in a cycle that produced both the high annealing temperature which will be encountered during the actual honeycomb panel braze cycle at a temperature of 1930 F and the age hardening (8 hours at a temperature of 1325 F) to be used during the panel attachment weld heat treat. Thus any metallurgical reactions which would occur in the segment would have been duplicated in the weld sample. Before mechanical test, a thin slice through the weld cross-sections of the specimen was removed for etching and micro-photography. Microscopic and fluorescent dye penetrant inspection of this section indicated that the electron beam did not completely contact the plating and the block on one of the four welds, producing incomplete fusion and penetration. As a result, a slightly wider beam will be used on the segment welds.

(U) The specimen was tested to failure between the platens of a testing machine. The imposed shear load simulates the load imposed on the weld by chamber pressure as shown in Fig.27 . Inspection of the parted sample indicated that diffusion bonding had occurred over part of the area between unwelded portions of the two blocks during the heat treat cycle. Corrections for this bonded area and the incomplete penetration of the fourth weld were made in the calculation of weld failure stress. The resulting ultimate weld shear strength was 40,000 psi; i.e., double the strength of nickel plating or one-fourth the strength of inconel 718. The plating layer exhibited excellent ductility and adhesion to the inner block. Thus the weld specimen test showed that the structural panel-to-baffle shear joint design was entirely adequate under the calculated load.

(U) Two subscale braze samples were prepared to check aspects of the planned honeycomb panel assembly braze cycle.(Fig. 28). In particular, the stack pressure, and alloy fillet size, wetting properties, and aggresive

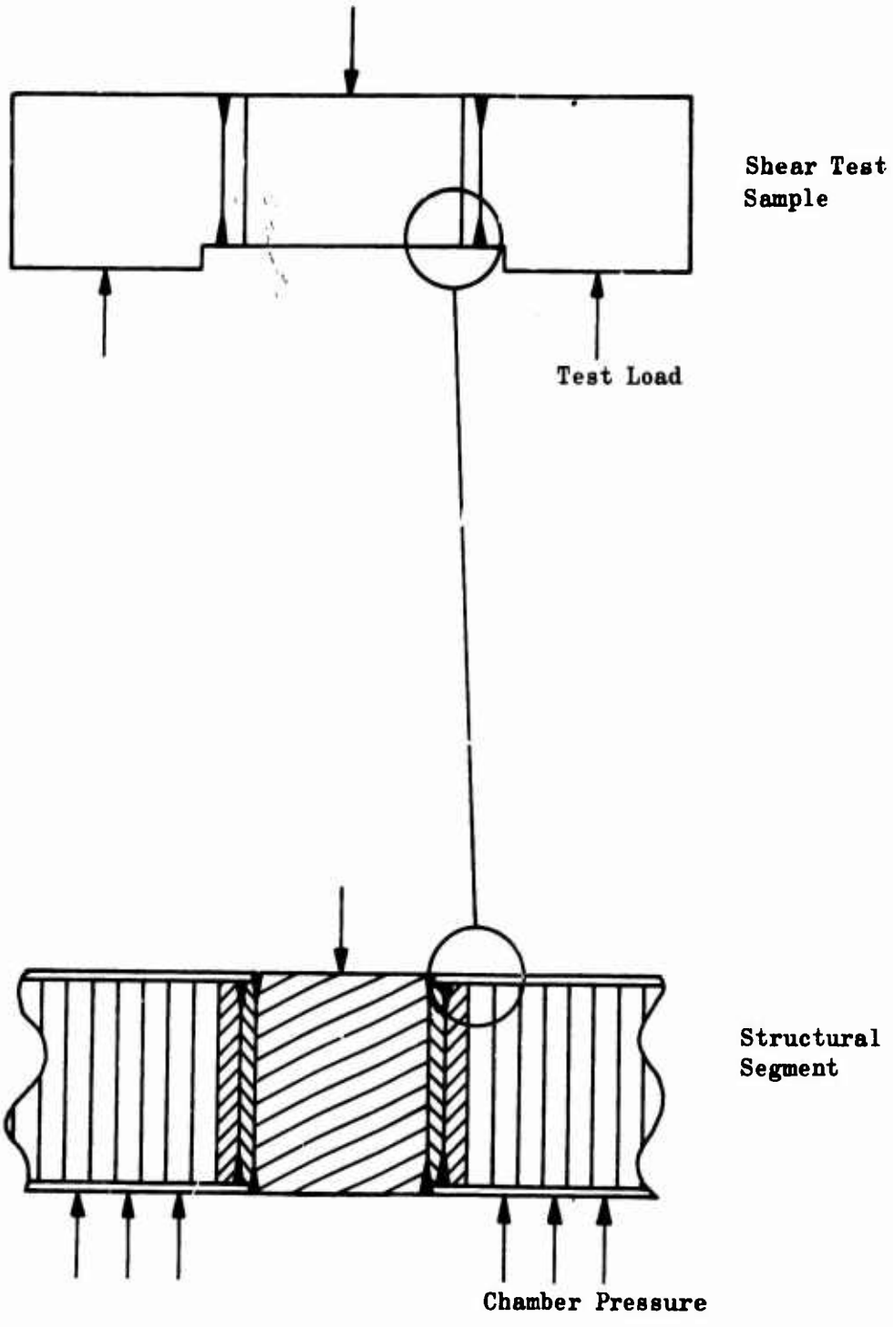

Figure 27 . Plated Edge Joint Weld Sample

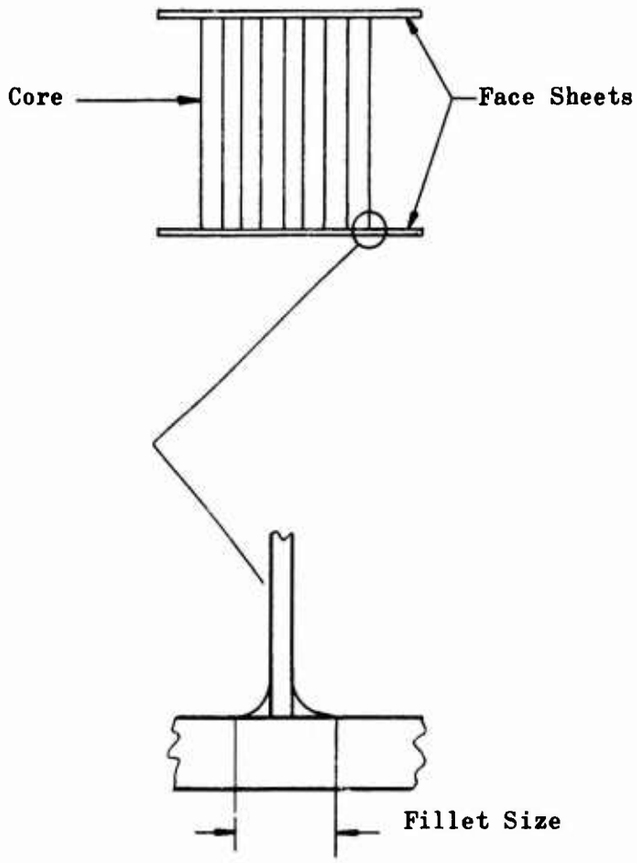

Figure 28 . Subscale Honeycomb Braze Samples

characteristics were of interest. Both full and subscale panel samples were brazed in an inner retort box having a thin sheet of metal foil welded over its top. By partially evacuating the retort, any pressure up to a full atmosphere could be applied through the foil to the honeycomb-sandwich assembly. Adequate pressure must be applied to ensure contact between the core and the braze alloy foil which was tack-welded to the face sheets. Excessive pressure must be avoided to prevent crushing the core. The pressure applied was scaled from that used during lower temperature honeycomb brazing at Los Angeles Division of North American Aviation. To ensure that air would not leak into the inert argon atmosphere in the inner retort, an outer retort was placed around the inner and filled with additional argon at atmospheric pressure.

(U) Shear strength data on the preferred braze alloy, Palniro No. 7, and two alternate alloys is shown in Fig.29 . One of the subscale braze samples employed Palniro No. 7 alloy with a thin plating of nickel on the brazed surfaces, the other used the same alloy without plating. These two samples resulted in good wetting characteristics and fillet size with no erosion of the thin-gage core foil in both subscale samples. Therefore, no specimens were brazed with alternate alloys. The thin nickel plating over the brazed surfaces did produce slightly better wetting of the surface, and was used on the full-scale panel sample. Micro sections prepared from both subscale samples indicated fillet sizes between 0.006 and 0.008 inch, which are adequate for the segment shear loads. A microsection of the nickel plated sample braze joint is shown in Fig. 30 .

(U) A full-size honeycomb panel was then brazed. This sample was intended to verify design factors that could not be checked at subscale; e.g. whether the fixtures to be used for the segment panels were adequate

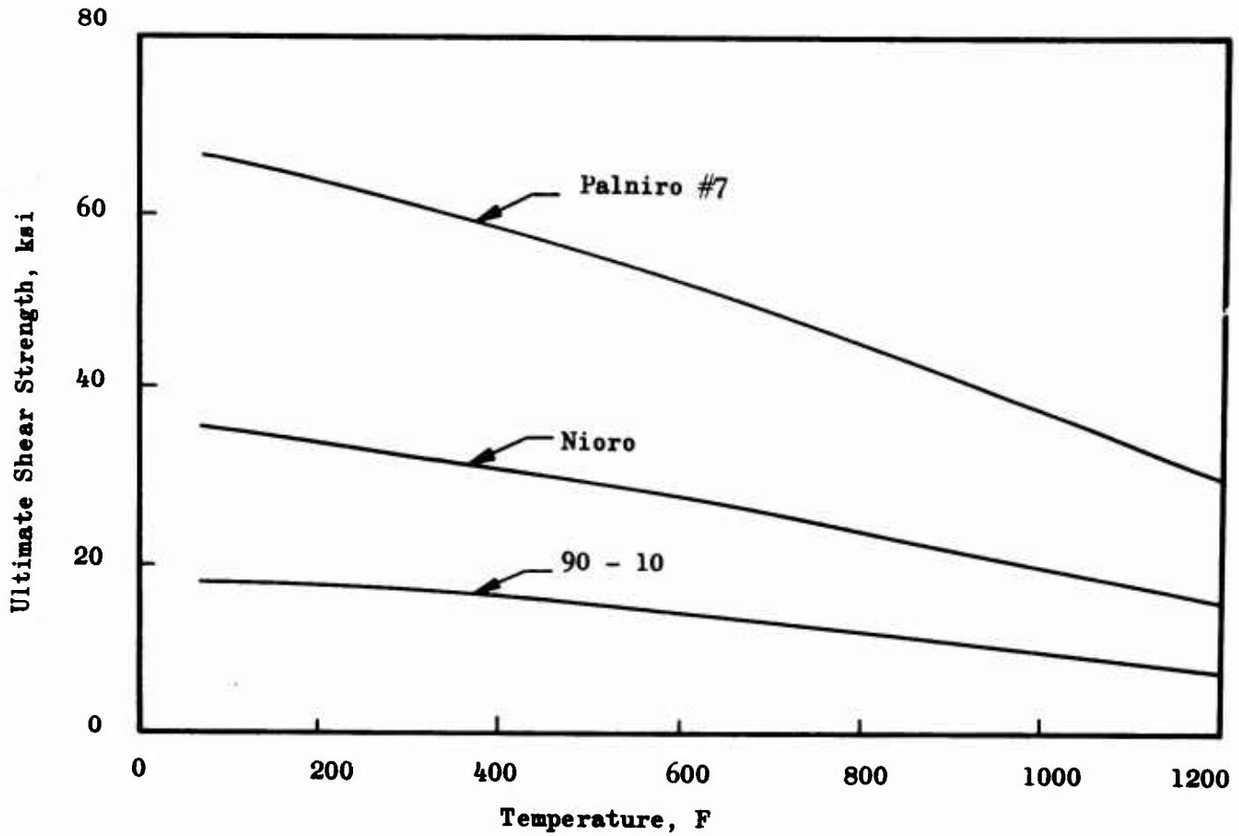

Figure 29 . Shear Strength of Candidate Braze Alloys

Figure 30. Face Sheet to Honeycomb Braze

to ensure braze bonds at all necessary points in the assembly. Chamfered plexiglas masks were fabricated to exclude nickel from unplated surfaces on the honeycomb core sections. Honeycomb panels with masks prior to plating are shown in Fig. 31 . Core edges were plated, machined off, and replated as was done with the plating sample. The replating cycle was terminated early on the sample core sections because of time limitations. The panel assembly, consisting of inner and outer face sheets, forward and aft core sections, and a splice sheet, was sandwiched between relatively thick upper and a lower form blocks of inconel 718 cut to the desired shape of the final panel.

(U) Diffusion bonding between form blocks and face sheets was prevented by placing stopoff-coated parting sheets of 0.010 thick CRES foil between them. Temperature and thermal gradients were monitored by three thermocouples. The first thermocouple was placed at the periphery of the assembly, the other two were inserted through machined ports to the centers of the upper and lower form blocks. Pressure was applied to the sandwich by partially evacuating the inner retort as with the subscale samples. The plated and brazed sample panel is shown in Fig. 32. A system of holes and grooves were machined into the form blocks to permit replacement of air with inert argon throughout the perforated core cells.

(U) Sectioning and ultrasonic inspection of the brazed panel revealed bonds at all necessary points except a small area between the outer face sheet and core near the splice sheet. A reduction of outer face-sheet bend radius together with provision for a chamfer on the core sections should result in complete bonding.

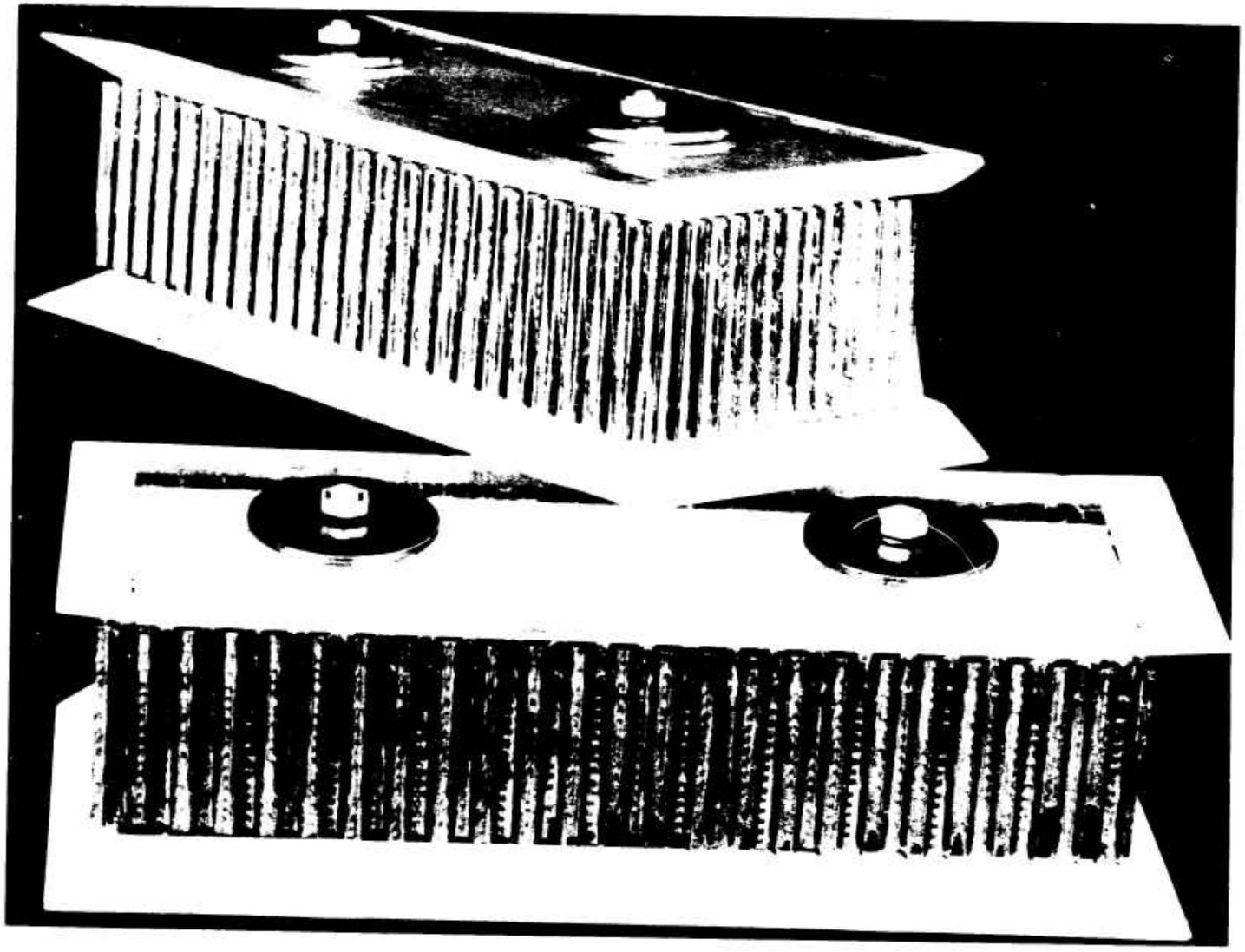

Figure 31 . Honeycomb Panels and Masks Prior to Nickel Plating

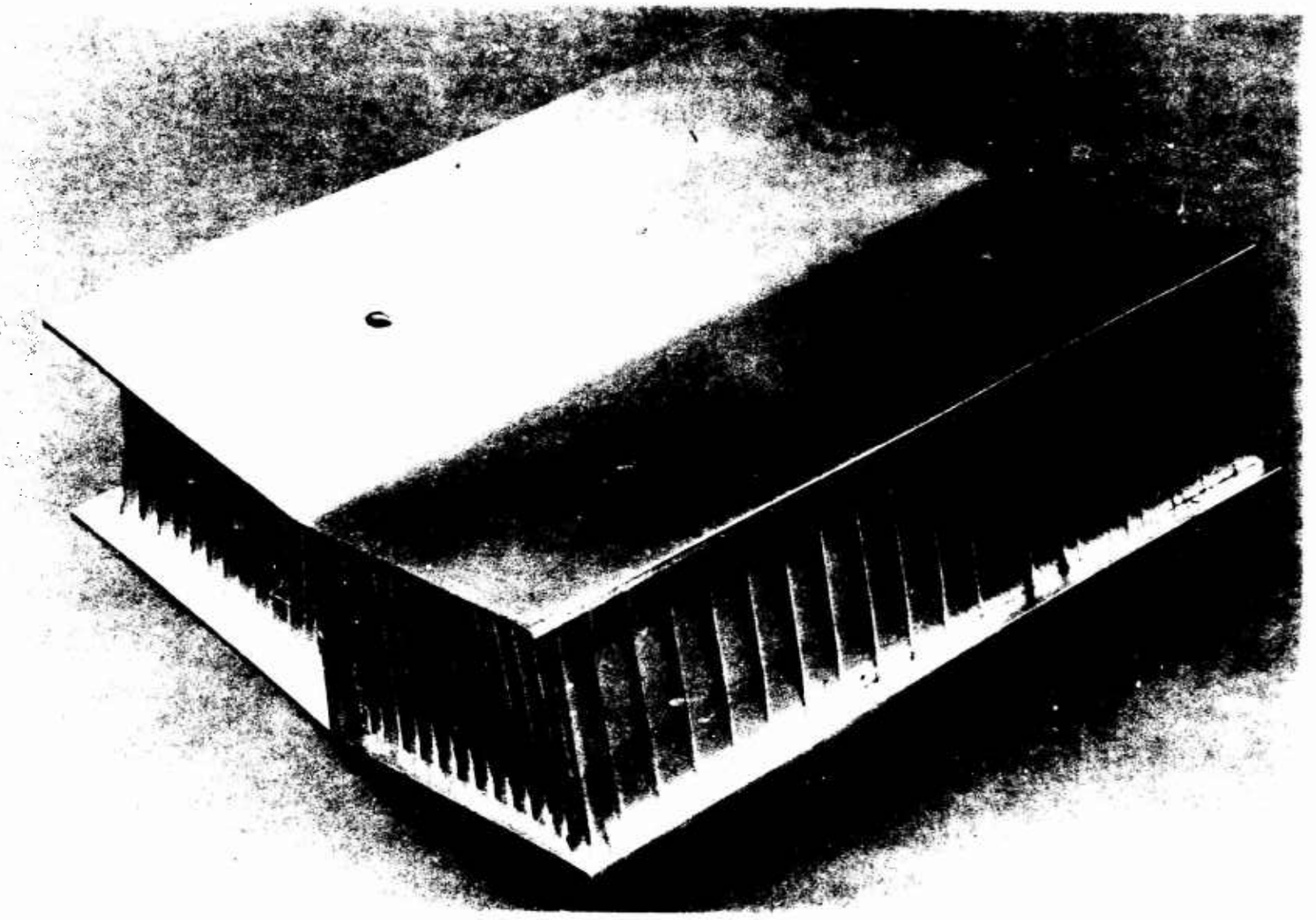

Figure 32 . Plated and Brazed Honeycomb Panel

SECTION V
EFFORT FOR THE NEXT QUARTER

(U) The major portion of the Task III effort will be completed during the next quarter. Both tube wall segments and the rib and honeycomb structural segments will complete fabrication. Mechanical testing of the structural segments and hot firing of the tube wall segments will also be completed. The effort remaining after the next quarter will be the test data analysis and final report preparation.

REFERENCES

1. Diem, H. G. Advanced Thrust Chamber for Space Maneuvering Propulsion, Task I System Studies Final Report, Rocketdyne, September, 1966, Confidential, AFRPL-TR-66-301

2. Diem, H.G. Advanced Thrust Chamber for Space Maneuvering Propulsion, First Quarterly Report, Contract AF04(611)-11617, Rocketdyne September, 1966, AFRPL-TR-66-232, Confidential

3. Diem, H.G. Advanced Thrust Chamber for Space Maneuvering Propulsion, Second Quarterly Report, Contract AF04(611)-11617, December, 1966, AFRPL-TR-66-338, Confidential

APPENDIX A

SOLID-WALL SEGMENT PERFORMANCE SUMMARY

(U) A summary of experimental results relating to performance of the solid-wall segments is given in Table A-1, in which the column headings refer to the following parameters:

Chamber:	one of the five chamber contours described in Table I
Triplet Injector:	1-B Triplet injector with 0.055 in dia GH_2 orifices
	1-B-1 Triplet injector 1-B with tapoff port
	3 Impinging Fan Injector (single row)
Duration:	time from attainment to 90 percent of chamber pressure to decay to 90 percent of chamber pressure
P_c	stagnation chamber pressure
$\dot{W}_T$	total propellant flowrate (excluding tapoff gas)
MR	mixture ratio, oxidizer/fuel(excluding tapoff gas)
F	measured thrust
A_t	geometric area of throat
C^*_{theo}	theoretical value of C* at listed P_c and MR
$(C^*)_p$	value of experimental C* based on P_c
(η_{C^*})	$(C^*)_p/C^*_{theo}$
$(C^*)_F$	value of experimental C* based on thrust
$(\eta_{C^*})_F$	$(C^*)_F/C^*_{theo}$

(U) Combustion chamber performance, η_{C^*}, is independently calculated based upon (1) chamber pressure and (2) thrust measurements. Performance based upon measured chamber pressure, throat area, and propellant flowrate is corrected for heat transfer, throat area changes caused by thermal expansion of the copper, the nozzle discharge coefficient, and the static/total chamber pressure ratio. Two LF_2 flowmeters in series and two or more (depending upon the hardware configuration) chamber pressure measurements are used.

TABLE A-1

PERFORMANCE DATA SUMMARY

Test No.	Chamber	Injector	Duration Seconds	Pc psia	F lb	$\dot{W}_T$ lb/sec	M.R	A_t in^2	C^*_{theo} ft/sec	ηC^*_p %	$(\eta C^*)_F$ %
100	E	3	3.4	299	163	0.633	14.2	0.468	8035	87.2	89.7
101	E	3	3.2	345	225	0.816	14.0	0.470	8077	89.0	89.6
102	E	3	3.2	431	249	0.829	13.2	0.470	8125	89.4	89.6
103	E	3	3.5	428	246	0.933	18.6	0.470	7817	87.0	86.3
104	E	3	3.7	428	245	0.897	16.1	0.470	7170	88.8	87.9
105	E	3	3.6	437	250	0.879	13.0	0.470	8136	90.7	90.3
106	E	3	3.8	301	163	0.629	13.9	0.470	8053	88.6	90.2
107	E	3	3.7	397	223	0.809	13.5	0.470	8103	90.0	90.0
108	E	1-B	3.2	319	185	0.621	13.4	0.470	8080	96.0	97.9
109	E	1-B	3.5	426	252	0.812	13.3	0.470	8118	96.8	96.3
110	E	1-B	3.5	480	286	0.910	13.3	0.470	8133	96.8	95.8
111	E	1-B	3.5	531	319	1.005	13.2	0.470	8150	96.4	95.3
112	E	1-B-1	3.6	411	*	0.792	14.1	0.468	8075	95.8	-
113	E	1-B-1	1.6	423	*	0.798	14.3	0.463	8070	98.0	-
114	E	1-B-1	3.5	425	*	0.807	13.4	0.468	8115	96.7	-
116	E	1-B-1	5.8	282	*	0.600	17.3	0.468	7860	90.3	-
117	E	1-B-1	5.8	274	*	0.593	15.7	0.468	7955	90.5	-
118	E	1-B-1	5.9	468	*	0.971	17.3	0.468	7930	91.5	-
129	E	1-B-1	5.8	353	*	0.703	13.3	0.468	8100	92.9	-
130	E	1-B-1	5.7	290	*	0.580	13.5	0.468	8065	93.5	-
131	E	1-B-1	5.7	483	*	0.971	14.7	0.468	8040	91.8	-

Tests 100 - 107; Conducted with non-optimized, single row impinging fan injector (Ref. 3)

Tests 108 - 111; Triplet injector characterization tests with oversized GH_2 injector orifices (Ref. 3)

Tests 112 - 131; Tests conducted with tapoff gas at various temperatures.

* Tapoff thrust effect not measured

CONFIDENTIAL

(U) For the thrust-based measurement, a specific impulse is determined from the thrust and propellant flowrates. The specific impulse is then used with the computed nozzle thrust coefficient to determine the combustion chamber efficiency. The theoretical ideal thrust coefficient is modified to account for such losses as drag, divergence, heat transfer, and chemical kinetic effects. More detailed descriptions of these corrections are given in Ref. 2 and 3. Very good agreement between the C* efficiencies based on thrust and chamber pressure measurements at the higher values of chamber pressure is shown in Table A-1. In the data presented in the previous quarterly report (Ref. 3) differences larger than 2 percent between the values of performance calculated by these two independent methods were found to exist on a number of tests. Because of the low thrust of the system, it is probable that the performance, C*, based upon chamber pressure is more accurate than the performance based upon thrust.

(C) One possible source of the difference between the values was the pressure on the base of the engine. A diagram of the base of the engine showing the aft closure ring and the angular position nomenclature is presented in Fig. A-1. Extensive data were accumulated on the pressure difference with respect to ambient pressure at various locations on the base for different thrust levels. The data are presented in Table A-2 and indicate that the base pressure was quite small, especially with the 15-degree exit angle chamber where the lower values are approaching the accuracy of the measurements. The pressure on the base of the ring was found to be approximately 0.03 psi. The data for the 30 degree exit nozzle indicates trends of increasing negative base pressure with increasing chamber pressure and proximity to the nozzle flow field. However, when the data are presented on the basis of a percentage contribution to the thrust, the base pressure effect varies from 0.5 to 1.0 percent with most of the data indicating a thrust reduction of 0.7 $\pm$ 0.1 percent resulting from aspiration of the base. Accordingly, this correction is included in the values of $\eta_{C^*_F}$ presented in Table A-1.

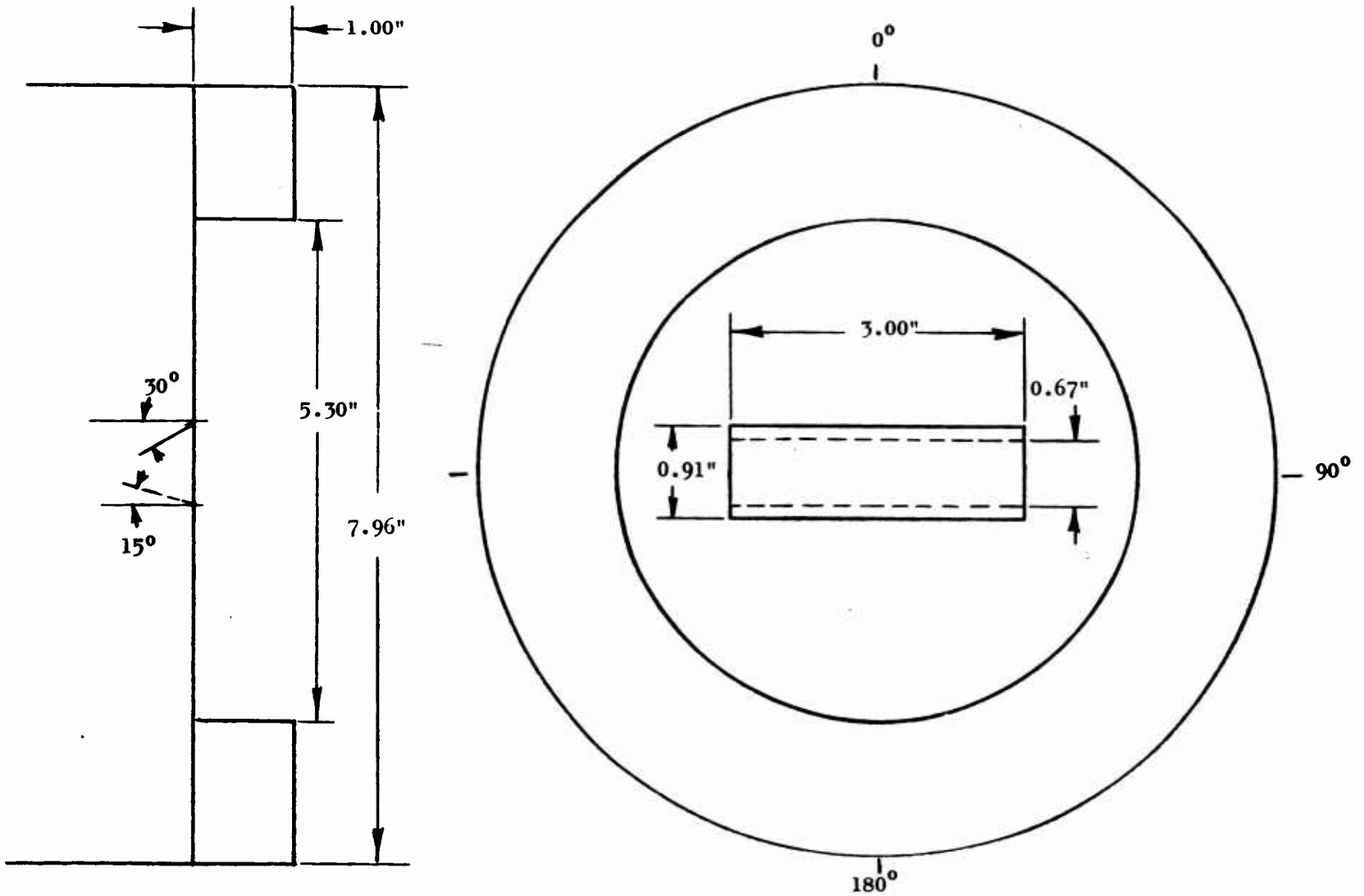

Figure A-1. Solid-Wall Segment Base

TABLE A-2

ENGINE BASE-PRESSURE DATA

Exit Angle deg.	Position Angle Deg.	Position Dist. From ℄, in.	P_c psia	P_{Base} psi (neg.)
15	0	0.75	300	0.05
			410	0.05
			360	0.05
			440	0.05
			420	0.04
15	0	1.5	430	0.02
			300	0.02
			380	0.02
			430	0.03
			480	0.03
			470	0.03
15	0	3.0	450	0.03
30	0	1.5	440	0.08
			460	0.08
30	0	3.0	510	0.05
			300	0.04
			440	0.05
			560	0.05
30	90	3.0	410	0.06
			500	0.07
			600	0.08
			320	0.06
			600	0.08

(C) In reviewing the data analysis methods, another source of the discrepancy was found in connection with the use of the pretest thrust zero used in the automatic data reduction process. The purpose of this measurement is to determine the forces acting on the load cell other than engine thrust so that these extraneous forces may be subtracted (or added depending upon direction) to the gross thrust reading during the test. It follows that only the extraneous forces, which do exist during the test, should be included in the pretest zero. To chill the injector and inlet plumbing prior to the test, LN_2 from a pressurized source is flowed through the injector. The LN_2 tank pressure is vented prior to the test. However, a review of the test records indicates that the pressure had not decayed completely at the time the pretest zeros were taken. The LN_2 flowing through the nozzle, therefore, imparts a thrust which is present at the time of the zero, but not present during the test. A calibration of the thrust resulting from the LN_2 flow vs the injector oxidizer manifold pressure is shown in Fig. A-2. This correction is generally in the order of 0.3 percent at full thrust but increases as the thrust level is reduced. The corrections were included in the performance presented in Table A-1.

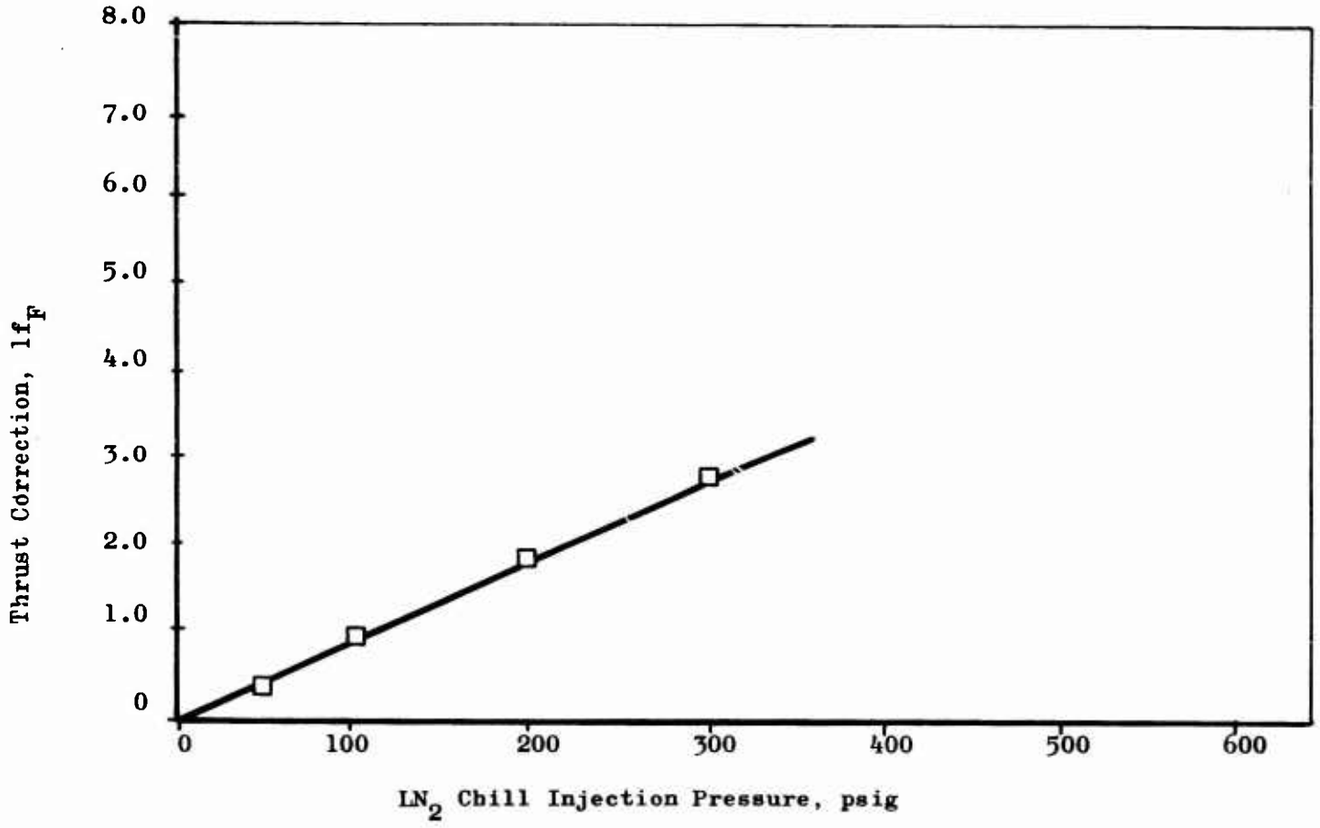

Figure A-2. Pretest Thrust Zero Correction for LN_2 Flow

APPENDIX B

TUBE-WALL GAS-SIDE TEMPERATURE

(U) The operating temperatures of the hydrogen coolant can be obtained by a solution of the following set of implicit equations. The required inputs are the gas-side film coefficient, the coolant flow conditions, and the wall resistance.

Wall Resistance:

$$T_{wc} = \frac{-a \pm \sqrt{a^2 + 2b\left(\frac{b}{2} T_{wg}^2 + a T_{wg} - x\, q/a\right)}}{b} \quad (1)$$

where $k = a + bT$

Gas-Side Film:

$$q/A = h_g (T_{aw} - T_{wg}) \quad (2)$$

Coolant Side Film:

$$q/A = h_c (T_{wc} - T_c) \quad (3)$$

Hydrogen Cooling Correlation: (4)

$$h_c = \rho V C_p \left(\frac{T_c}{T_{wc}}\right)^{0.55} \frac{f/2}{0.92 + \sqrt{f/2}\left[G(\epsilon^*, Pr) - 8.48\right]}$$

where

$$G(e^*, Pr) = 4.5 + 0.57 (e^*)^{0.75} \qquad 0 \le e^* \le 7$$

$$G(e^*, Pr) = 5.7 (e^*)^{0.2} \qquad e^* > 7$$

$$e^* = Re \frac{e}{di} (f/2)^{0.5}$$

NOMENCLATURE

k	thermal conductivity, Btu/in-F
a,b	thermal conductivity temperature sensitivity constants
x	tube wall thickness, in.
q/a	heat flux, Btu/in^2 sec
hg	gas side film coefficient, Btu/in^2 sec F
hc	liquid side film coefficient, Btu/in^2sec F
T_{wc}	coolant side tube wall temperature, F
T_{wg}	gas side tube wall temperature, F
Tc	coolant bulk temperature, F
ρ	coolant bulk density, lb/in^3
V	coolant velocity, in^2/sec
C_p	coolant specific heat, Btu/lb F
f	function factor
G	mass flowrate, lb/sec in^2
ϵ	tube inside surface roughness, microinches
Pr	Prandtl number
Re	Reynolds number
d_i	tube inside diamter

Unclassified

Security Classification

DOCUMENT CONTROL DATA - R&D

(Security classification of title, body of abstract and indexing annotation must be entered when the overall report is classified)

1. ORIGINATING ACTIVITY *(Corporate author)*
Rocketdyne, a Division of North American Aviation, Inc. 6633 Canoga Ave., Canoga Park, California

2a. REPORT SECURITY CLASSIFICATION
CONFIDENTIAL

2b GROUP 4

3. REPORT TITLE

(Unclassified Title)
ADVANCED THRUST CHAMBER FOR SPACE MANEUVERING PROPULSION

4. DESCRIPTIVE NOTES *(Type of report and inclusive dates)*
Third Quarterly Report 16 November to 15 February 1966

5. AUTHOR(S) *(Last name, first name, initial)*
Diem, H.G.

6. REPORT DATE	7a. TOTAL NO. OF PAGES	7b. NO. OF REFS
March 1966	88	4

8a. CONTRACT OR GRANT NO.	9a. ORIGINATOR'S REPORT NUMBER(S)
AF04(611)-11617	R-6727-3
b. PROJECT NO.	
c.	9b. OTHER REPORT NO(S) *(Any other numbers that may be assigned this report)* AFRPL-TR-67-78
d.	

10. AVAILABILITY/LIMITATION NOTICES
In addition to security requirements which must be met, this document is subject to special export controls and each transmittal to foreign governments or foreign nationals may be made only with prior approval of AFRPL, Edwards, California 93523

11. SUPPLEMENTARY NOTES	12. SPONSORING MILITARY ACTIVITY
	Air Force Rocket Propulsion Laboratory Research and Technology Division Edwards, California

13. ABSTRACT

Hardware design, fabrication and hot-firing test results for toroidal thrust chamber segments are discussed. Solid-wall segment testing has been conducted to evaluate injector and thrust chamber contour designs with respect to performance and heat transfer. Fabrication status of tube-wall throat inserts, tube wall segments, and structural test segments are presented. Hot firing test results for a tube wall throat insert are discussed.

DD FORM 1 JAN 64 1473

Unclassified

Security Classification

Unclassified

Security Classification

14. KEY WORDS	LINK A		LINK B		LINK C	
	ROLE	WT	ROLE	WT	ROLE	WT
Fluorine/Hydrogen Propellants						
Advanced Thrust Chamber						
Throttling						
Testing						
Segments						

INSTRUCTIONS

1. ORIGINATING ACTIVITY: Enter the name and address of the contractor, subcontractor, grantee, Department of Defense activity or other organization *(corporate author)* issuing the report.

2a. REPORT SECURITY CLASSIFICATION: Enter the overall security classification of the report. Indicate whether "Restricted Data" is included. Marking is to be in accordance with appropriate security regulations.

2b. GROUP: Automatic downgrading is specified in DoD Directive 5200.10 and Armed Forces Industrial Manual. Enter the group number. Also, when applicable, show that optional markings have been used for Group 3 and Group 4 as authorized.

3. REPORT TITLE: Enter the complete report title in all capital letters. Titles in all cases should be unclassified. If a meaningful title cannot be selected without classification, show title classification in all capitals in parenthesis immediately following the title.

4. DESCRIPTIVE NOTES: If appropriate, enter the type of report, e.g., interim, progress, summary, annual, or final. Give the inclusive dates when a specific reporting period is covered.

5. AUTHOR(S): Enter the name(s) of author(s) as shown on or in the report. Enter last name, first name, middle initial. If military, show rank and branch of service. The name of the principal author is an absolute minimum requirement.

6. REPORT DATE: Enter the date of the report as day, month, year; or month, year. If more than one date appears on the report, use date of publication.

7a. TOTAL NUMBER OF PAGES: The total page count should follow normal pagination procedures, i.e., enter the number of pages containing information.

7b. NUMBER OF REFERENCES: Enter the total number of references cited in the report.

8a. CONTRACT OR GRANT NUMBER: If appropriate, enter the applicable number of the contract or grant under which the report was written.

8b, 8c, & 8d. PROJECT NUMBER: Enter the appropriate military department identification, such as project number, subproject number, system numbers, task number, etc.

9a. ORIGINATOR'S REPORT NUMBER(S): Enter the official report number by which the document will be identified and controlled by the originating activity. This number must be unique to this report.

9b. OTHER REPORT NUMBER(S): If the report has been assigned any other report numbers *(either by the originator or by the sponsor)*, also enter this number(s).

10. AVAILABILITY/LIMITATION NOTICES: Enter any limitations on further dissemination of the report, other than those imposed by security classification, using standard statements such as:

(1) "Qualified requesters may obtain copies of this report from DDC."

(2) "Foreign announcement and dissemination of this report by DDC is not authorized."

(3) "U. S. Government agencies may obtain copies of this report directly from DDC. Other qualified DDC users shall request through _____."

(4) "U. S. military agencies may obtain copies of this report directly from DDC. Other qualified users shall request through _____."

(5) "All distribution of this report is controlled. Qualified DDC users shall request through _____."

If the report has been furnished to the Office of Technical Services, Department of Commerce, for sale to the public, indicate this fact and enter the price, if known.

11. SUPPLEMENTARY NOTES: Use for additional explanatory notes.

12. SPONSORING MILITARY ACTIVITY: Enter the name of the departmental project office or laboratory sponsoring *(paying for)* the research and development. Include address.

13. ABSTRACT: Enter an abstract giving a brief and factual summary of the document indicative of the report, even though it may also appear elsewhere in the body of the technical report. If additional space is required, a continuation sheet shall be attached.

It is highly desirable that the abstract of classified reports be unclassified. Each paragraph of the abstract shall end with an indication of the military security classification of the information in the paragraph, represented as *(TS)*, *(S)*, *(C)*, or *(U)*.

There is no limitation on the length of the abstract. However, the suggested length is from 150 to 225 words.

14. KEY WORDS: Key words are technically meaningful terms or short phrases that characterize a report and may be used as index entries for cataloging the report. Key words must be selected so that no security classification is required. Identifiers, such as equipment model designation, trade name, military project code name, geographic location, may be used as key words but will be followed by an indication of technical context. The assignment of links, rules, and weights is optional.

Unclassified

Security Classification